Three-dimensionally deformable, highly stretchable, permeable, durable and washable fabric circuit boards

Qiao Li[1], and Xiao Ming Tao [1,2]

[1]Institute of Textiles and Clothing, and [2]Interdisciplinary Division of Biomechanical Engineering, The Hong Kong Polytechnic University, Hong Kong, China

Abstract

This paper reports fabric circuit boards (FCBs), a new type of circuit boards, that are three-dimensionally deformable, highly stretchable, durable and washable ideally for wearable electronic applications. Fabricated by using computerized knitting technologies at ambient dry conditions, the resultant knitted FCBs exhibit outstanding electrical stability with less than 1% relative resistance change up to 300% strain in unidirectional tensile test or 150% membrane strain in three-dimensional ball punch test, extraordinary fatigue life of more than 1 000 000 loading cycles at 20% maximum strain, and satisfactory washing capability up to 30 times. To the best of our knowledge, the performance of new FCBs has far exceeded those of previously reported metal-coated elastomeric films or other organic materials in terms of changes in electrical resistance, stretchability, fatigue life and washing capability as well as permeability. Theoretical analysis and numerical simulation illustrate that the structural conversion of knitted fabrics is attributed to the effective mitigation of strain in the conductive metal fibres, hence the outstanding mechanical and electrical properties. Those distinctive features make the FCBs particularly suitable for next-to-skin electronic devices. This paper has further demonstrated the application potential of the knitted FCBs in smart protective apparel for *in situ* measurement during ballistic impact.

1. Introduction

Applications of wearable electronic devices place great demands on fibre-based devices and circuit board assemblies that are in direct contact with the soft, three-dimensional and extensible (from 3% to 55% strain) human body [1–5]. Such next-to-skin electronic assemblies require a new family of flexible and stretchable circuit boards that work in repeated large deformation in the tensile, bending and shear modes and in three dimensions [6–8]. The circuit boards should have low moduli comparable to those of human tissues such as skin and muscles;

they need to be permeable, comfortable to wearers and washable [9]. Fabric circuit boards (FCBs), therefore, have enormous potential to fit such a purpose. FCBs mechanically support and electrically connect discrete electronic components by using conductive tracks or others made from electrically conductive fibrous materials of metal, conductive polymers or composites, prints or coatings, supported by dielectric fibrous structures [10,11]. FCB technologies, instead of cumbersome cables which inevitably restrict certain movements [12–17], enable the whole FCB assembly to be worn on three-dimensional human bodies in real daily activities [18], thereby opening up a large number of potential applications such as electronic skins [19,20], conformable sensor networks (or arrays) on human bodies [10,21–24] and biointegrated systems for health monitoring or therapeutic purposes [16,25–29].

Similar to printed circuit boards, FCBs can be designed with single-, double- or multi-layered structures (electronic supplementary material, figure S1). They are fabricated by computer-integrated manufacturing technologies, including weaving [30–35], knitting [36], stitching [37] or embroidering [38–40] of fine conductive fibres (e.g. stainless steel yarn [41,42], silver-plated polyamide filament [38], copper fibre [43–45]) into fabrics [2,38,46]. FCBs can also be made by printing [47–49] or coating conductive materials (e.g. conductive elastomers [50–58], carbon-filled rubbers [59], conductive carbon nanotube (CNT) or AgNW inks [60,61]) on fabrics or paper substrates instead of copper laminated polymer film substrates [62,63]. Lamination of fabrics with thin metal films is an alternative approach [63]. Of the above-mentioned three, the first approach has the potential for the real wearable FCBs that meet all the above-mentioned performance requirements.

As a family member of circuit boards, FCBs should possess excellent electrical conductivity and appropriate current carrying capacity, high thermo-electromechanical reliability and safety, electromagnetic compliance at high frequency (more than 30 MHz) as well as good connectivity for techniques such as surface mounting technology. Primarily designed for wearable applications, FCBs have additional key property requirements, that is, air permeability; three-dimensional deformability in single or mixed modes of bending, compression, extension and shear; electrical and mechanical integrity over large deformation with tensile strain as large as 60%; fatigue life of over one million loading cycles; washing capability of over 30 washing cycles.

To date, woven and printed FCBs have been studied to physically link various distributed electronic components with the functions of sensing, monitoring and information-processing,

such as wearable motherboard [58,64,65], sensorized gloves [50,56,66] and intelligent knee sleeves [67,68], driving the initial step towards wearable applications coverable human bodies due to their inherently mechanical drapability and foldability. However, the woven/non-woven and embroidered/stitched FCBs have failed mechanically and electrically within 20–30% strain [31]; printed conductive tracks have suffered inconvenient cracks when subjected to bending or stretching deformation modes [69].

Alternative technologies represented by novel organic materials [19,70–77] and wavy metal films [78–82] or buckled semiconductor nanoribbons [83–93] on compliant substrates have pushed electronic components, interconnects, as well as integrated circuits towards out-of-planar possibilities where bending and stretching deformation modes may dominate [94]. Organic materials such as (well-controlled) graphene particles [19,70,71], CNT composites [72–74,95], polyaniline-conducting polymer [75] as well as PEDOT–PSS composites [76] yield different stretching levels (ranging from several per cent to more than 100%) through blending with silicone rubbers (e.g. PDMS). The conductivity for those organic elastic conductors, except MWNT/Ag composite (conductivity: 3700 $S\,cm^{-1}$) [73], is too low (conductivity: less than 1000 $S\,cm^{-1}$) to perform as electrical wirings, particularly for integrated circuits [96–98]. More crucially, most of such organic conductors, except polymeric ionic conductors [99], drop their conductivity by at least several orders of magnitude even within 10% strain [75]. In contrast, metal films (e.g. Au, Ag and Cu) with comparatively high conductivity and semiconductor (e.g. SiO_2 and Ge) nanoribbons on elastic substrates are capable of being stretched by means of mechanically optimized structural configurations. They have been evaluated from aspects of stretchability, fatigue life and relative change in electrical resistance during deformation. Net-shaped gold-coated elastomer film stretched by adjusting its struts achieved 2000 cycles under 20% strain with about 60% rise in its electrical resistance [19,20]. Microcracked gold film on the PDMS substrate, created by thermal expansion mismatch, endured 25 000 cycles at 20% strain, while increasing its electrical resistance by 300% [100]. Horseshoe copper film embedded in the PDMS substrate, with a fatigue life of 2500 cycles at 10% strain, was capable of being stretched up to 56% strain with an increment of 2.1% in its electrical resistance [101]. Controlled wrinkling semiconductor nanoribbons on the PDMS substrates, from thin silicon ribbon with a wavy shape [84,85], to a pop-up pattern [83,102,103], non-coplanar mesh [86,89], as well as non-coplanar mesh with serpentine bridges [90–92], have increased their stretchability from 10% to 140% owing to the out-of-plane deflection in thin layers, thereby accommodating strains applied in the plane. Despite the

boosted stretchability by a series of elaborate mechanical optimizations, electrical integrity in the stretching process and durability for both organic and inorganic electronics are still far from the requirements in real wearable applications. What is more, next-to-skin electronics demands elastic substrates to be breathable, with the ability of transferring heat and moisture or water vapour, and washable for repeated usage [43].

In this paper, we extend our previous work on knitted electrical interconnects [36] to a knitted FCB technology, which offers a set of properties that is not effective with woven, rigid or elastomeric circuit boards. The FCB (i) is capable of being stretched beyond 300% strain with an appropriate current carrying capacity of 15 mA owing to its three-dimensionally looped configuration and the way in which neighbouring loops fit together; (ii) is soft with a low elastic modulus (approx. 350 kPa), near to that of human skin (less than 1 MPa); (iii) is porous (air permeability: from 0.003 to 0.158 kPa s m^{-1}), which is a vital concern for the comfort of the product next to the stratum corneum, the most superficial layer of the human skin; (iv) is durable with long fatigue life over 1 000 000 loading cycles at 20% maximum strain; and (v) can be washed more than 30 times. A prototype of FCB assembly in the form of a fabric sensing network, in which fabric strain sensor arrays are electrically linked and mechanically supported by the developed knitted FCB, is then demonstrated for wearable electronic applications.

2. Results

We produced FCB samples by incorporating polyurethane-coated copper fibres, together with pre-stretched (approx. 150%), elastic filament yarns into a single jersey-knitted fabric in three-dimensional hooked (or looped) configurations on a computerized knitting machine (electronic supplementary material, figure S4*b*). The yarn has a composite structure with highly segmented polyurethane filaments (diameter: 40 μm, 2f) in the core and textured polyamide multifilaments (diameter: 40 μm, 24f) wrapped around the core (electronic supplementary material, figure S3*c*). Figure 1 shows images from optical microscopy and scanning electron microscopy (SEM) of the resultant sample. Figure 1*a* illustrates the microstructure of knitted FCB around the nail (radius of curvature at the nail tip: approx. 1 mm) of a little finger (radius: approx. 60 mm). Figure 1*b*–*f* shows SEM images of a knitted FCB in a dry relaxed state. One typical conductive track in the FCB consists of two polyurethane-coated metal fibres (core diameter: approx. 50 μm; coating thickness: approx. 3 μm) with a series of connected three-dimensional loops in which the circular portions at the two ends are out-of-plane (height of the loop: approx. 180 μm; period of the loop: approx. 800 μm) and the straight segments, penetrating into the

knitted fabric, are interlaced with the elastic textile yarns (figure 1*b–d*). The metal fibre loops, whose density in the knitted FCB is 10 loops cm^{-1}, are closely arranged with uniform loop length (the length of the metal fibres in a single loop, approx. 5200 μm), period (the minimum distance between two adjacent loops, approx. 850 μm) and amplitude (the maximum distance from the trough to the crest, approx. 1720 μm; figure 1*b*). The thickness of the single jersey-knitted fabric board is 800 μm; the mass per unit area is 160 g m^{-2}, and the density is 10 loops cm^{-1} in both transverse and longitudinal directions (figure 1*c*). SEM micrographs in figure 1*e–f* show the coated metal fibre, whose surface is smooth, remains intact after being incorporated into the knitted fabric through the knitting process. The copper fibre of 50 μm core diameter is coated by a polyurethane film with 3 μm thickness. The advantages of the coating are (i) the metal fibre is insulated, avoiding short circuits when two adjacent loops contact each other [104]; (ii) the metal fibre is protected from the chemical or environmental attacks, so that it is unnecessary to further encapsulate the resulting FCB, without the risk of reducing its stretchability for practical applications [105,106]; (iii) the fine metal fibre, with reduced bending ($\pi d^4E/64 \approx 7.85e(-5)$ N mm^2) and torsional rigidities ($\pi d^4G/32 \approx 5.95e(-5)$ N mm^2) as well as enhanced mechanical robustness (breaking strain: 16%) owing to a thin and compliant protection can be deformed substantially to three-dimensionally looped configurations (electronic supplementary material, figure 3*b*). Apart from the fibre coating, the metal fibres are completely covered by polyamide multifilaments from the front side view of the knitted FCB (figure 1*c*) owing to the pre-stretched spandex filaments, which then shrink to their original states when free of external force after the manufacturing process. Such porous fibrous structures can be worn directly on human bodies, without irritating skin during long-term use. Additionally, compression and friction during wear can be mitigated if the knitted FCB has its front side towards the human body.

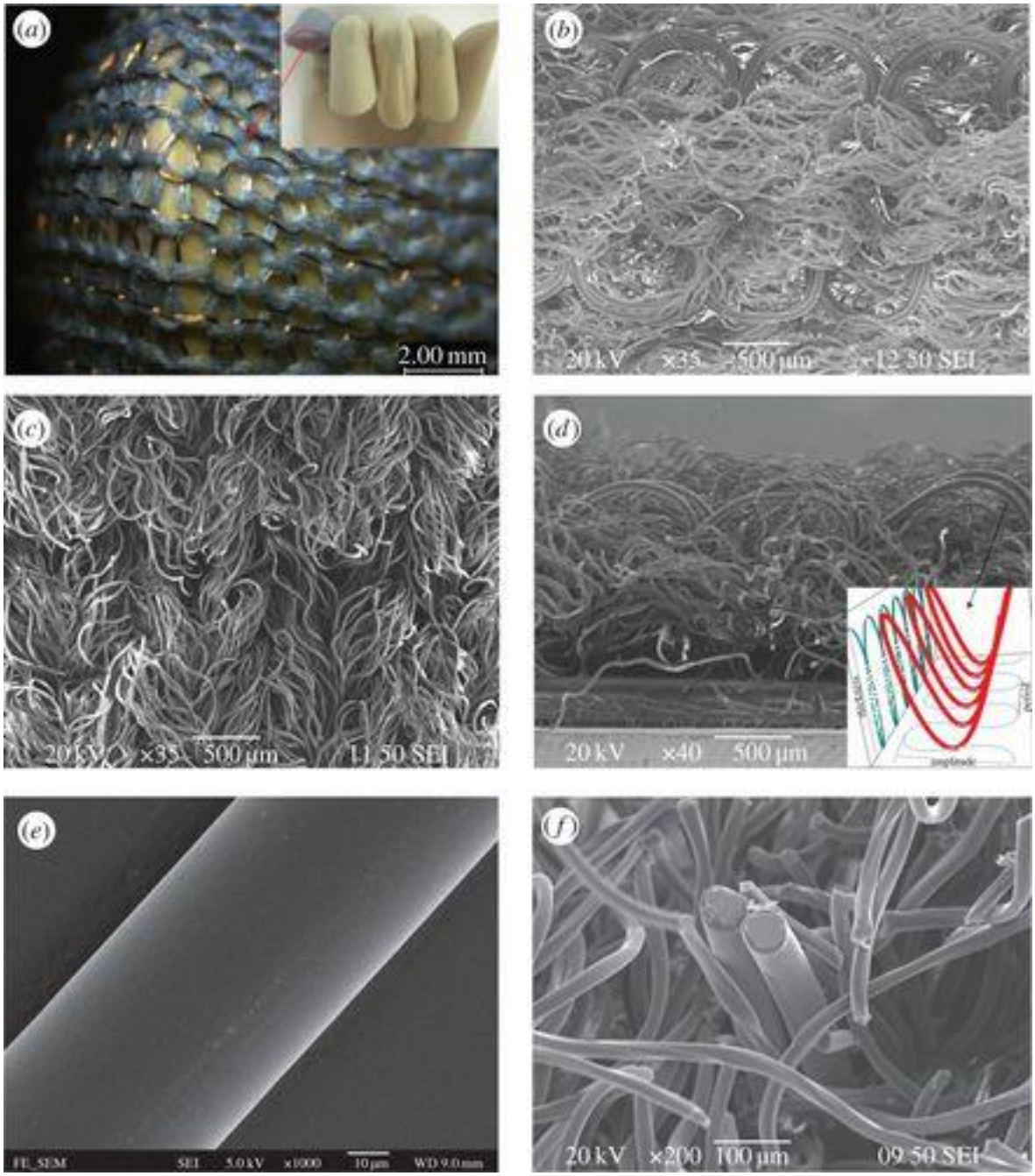

Figure 1. Structure of a knitted FCB. (*a*) Optical image of one stretched FCB on a human finger. (*b–d*) Backside, front-side and cross-sectional views of the FCB. (*e*,*f*) SEM images of the coated metal fibres (core diameter: approx. 50 μm; coating thickness: approx. 3 μm). (Online version in colour.)

The three-dimensional-looped configuration of the metal fibres and their interlaced integration with the smooth, compliant textile yarns facilitate a large reduction in their peak strain, because of structural conversion in single jersey-knitted fabrics that leads to less than 1% even if the knitted fabric is stretched over 60% [1,107]. Because fatigue life is known to be related

inversely to strain level exponentially, the resistance to fatigue of the knitted FCB during repeated deformation cycles can be greatly enhanced and its electrical integrity can be well preserved [36]. The resistance of one electrical conductive track in the resultant-knitted FCB was monitored while it was being stretched to mechanical and electrical failures. The electrical resistance of the track in the FCB of 2.5×7 cm (gauge length: 5 cm) is approximately 3.9 Ω and remains constant ($(R-R_0)/R_0 \approx 0$) when it is unidirectionally stretched up to 300% strain in either transverse (course) or longitudinal (wale) direction (figure 2*a*). The knitted FCB has a Young's modulus of approximately 30 kPa and approximately 40 kPa in the transverse and longitudinal directions, respectively (electronic supplementary material, figure S4*d*). The metal fibres are first unbent in the transverse tensile test then stretched by the interlaced filament yarns. In the longitudinal direction, the metal fibres are further bent and pulled from their horizontal segments into the v-segments then stretched with applied strain [41]. As the strain further increases over 300%, the resistance starts to increase monotonically, similar to the resistance–strain curve of the free-standing polyurethane-coated metal fibre (electronic supplementary material, figure S3*b*). Relative change in electrical resistance and stretchability of others' work is summarized in figure 2*b* [115]. The stretchability has been increased by either structural conversion or using organic materials from approximately 3% (SiNW on PDMS substrate [110]) to more than approximately 400% (wrinkled graphene on PDMS substrate [71]). The relative change in electrical resistance varies from approximately 2.1% (horseshoe pattern on PDMS substrate [108]) to approximately 7300% (Ag-MWNT-SIS nanocomposite film [73]), which may hinder the use as conductive tracks in stretchable circuit boards, in particular, for low-impedance electronic components or high-precision measurements [96,97]. By contrast, the knitted FCB has exhibited an extraordinarily electrical stability with almost no change in electrical resistance up to strain of 300% in unidirectional tensile deformation.

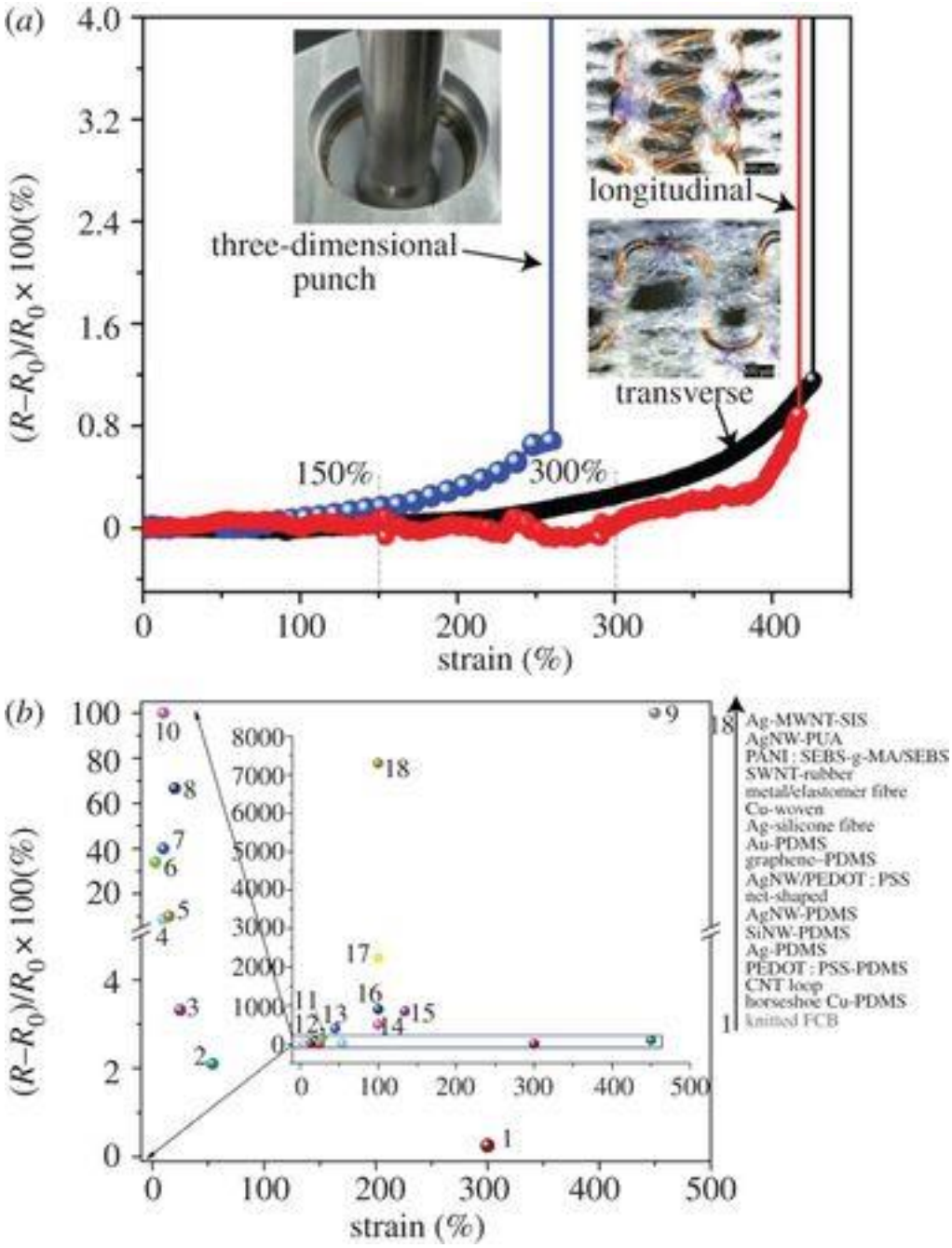

Figure 2. Relative resistance change as functions of strain. (*a*) Relative resistance change–strain relation of one conductive track in the knitted FCB in tensile and three-dimensional punch tests. (*b*) Comparison with others' work (2, horseshoe Cu–PDMS [108]; 3, CNT loop [74]; 4, PEDOT : PSS–PDMS [76]; 5, Ag–PDMS [109]; 6, SiNW–PDMS [110]; 7, AgNW–PDMS [111]; 8, net-shaped [20]; 9, AgNW/PEDOT : PSS [112]; 10, graphene–PDMS [71]; 11, Au–PDMS [82]; 12, Ag–silicone fibre [96]; 13, Cu-woven [2]; 14, metal/elastomer fibre

[113]; 15, SWNT–rubber [72]; 16, PANI : SEBS-g-MA/SEBS [75]; 17, AgNW–PUA [114]; 18, Ag-MWNT-SIS [73]).

Knitted fabrics can easily form a double-curvature drape owing to their excellent bending, shear and membrane stretch behaviour. To examine three-dimensional deformability, a ball punch test was conducted, where a polished stainless steel ball (diameter: approx. 25.4 mm) was punched into an FCB sample, the same as the samples used for the unidirectional tensile test, at 90° (electronic supplementary material, figure S4*c*) [36]. Figure 2*a* and electronic supplementary material, figure S4*d* present the relative resistance change and stress of the knitted FCB as functions of calculated average membrane strain [36]. The FCB exhibits a constant electrical resistance until being stretched over an average membrane strain of 150%, which is one half of breaking elongation of the knitted FCB. The comparatively reduced stretchability (approx. 150%) in the three-dimensional punch test may be attributed to the complex deformation mode, including fibre bending, lateral compression, torsion and axial tension as well as compression and friction between the knitted FCB and stainless steel ball. The knitted FCB, owing to its significant three-dimensional deformability, excellent electrical integrity, as well as softness and permeability, is the most feasible for application in next-to-skin electronics.

To reveal the underlying mechanism that contributes to outstanding mechanical deformability with electrical integrity, we examined the structural change of the three-dimensionally looped metal fibres in the soft-knitted FCB. SEM images in figure 3*a–d* show several representative geometrical configurations of the knitted FCB in various deformed states, either transversely or longitudinally. The metal fibre loops slide and adjust their geometrical parameters, i.e. period and amplitude, by means of straightening in the transverse case, whereas bending to the smaller radius of curvature in the longitudinal direction, hence accommodating the applied deformation. Figure 3*e–f* plots the measured period and amplitude of metal fibre loops as functions of applied strain in the transverse, longitudinal unidirectional tensile tests, as well as the ball punch test. The data were obtained from at least 10 optical images (electronic supplementary material, figure S5). In the transverse case, the period increased consistently from 0.85(±0.01) to 2.89(±0.04) mm, in approximately linear fashion proportional to applied strain; the amplitude, on the other hand, decreased to 1.07(±0.02) mm at 300% strain from an initial amplitude of 1.72(±0.04) mm. In contrast, there was a reduction in the period to 0.51(±0.01) mm and an increment in the amplitude to 2.20(±0.01) mm with applied strain up

to 300% in the longitudinal direction. Unlike unidirectional tensile tests, the ball punch test shows complex adjustments in the period and amplitude, hinting that much larger fibre strain might be induced.

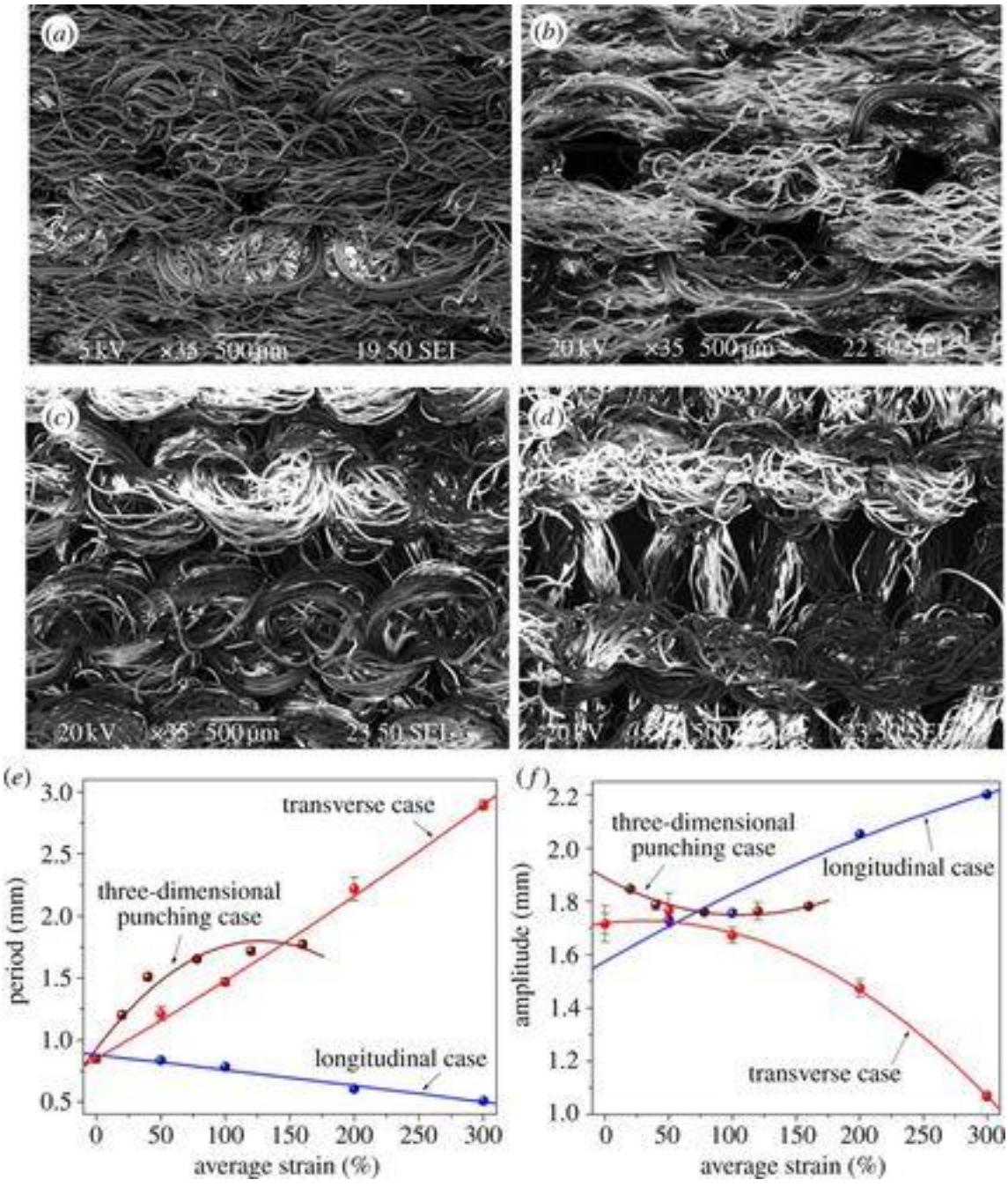

Figure 3. Geometrical change of the knitted FCB in transverse and longitudinal tensile tests. (*a*,*b*) SEM images at 60% and 120% strain in the transverse direction, respectively. (*c*,*d*) SEM images for 60% and 120% in the longitudinal case. (*e*,*f*) Corresponding period and amplitude with applied strain.

Further observation suggests that conductive tracks in the knitted FCB are stretched to a flat geometry as the applied tensile strain increases. The combination of out-of-plane and in-plane deformation of the three-dimensional loops accommodates the large FCB deformation in a way that avoids any significant local strain of the metal fibres, enhancing electrical integrity. Further stretching may produce larger tensile strain to the flat metal fibre loops, resulting in their breaking when the failure strain of the free-standing metal fibres is reached.

Wearable applications demand flexible and stretchable electronics to be mechanically and electrically robust with sufficient fatigue life. The Coffin–Manson law was applied for predicting fatigue life N of the knitted FCB. To derive two constants A=1.025e(−20) and B=−11.92 in equation $N=A\varepsilon^{B}_{\text{fibre}}$, where $\varepsilon_{\text{fibre}}$ was the simulated peak strain of the metal fibre with practical elongation of the FCB (electronic supplementary material, figure S7), we examined the variation of electrical resistance when two to three specimens were subjected to a cyclic tensile test at a maximum FCB elongation of 60% ($\varepsilon_{\text{fibre}}$=0.008) and 80% ($\varepsilon_{\text{fibre}}$=0.01) in the transverse direction. According to the above-mentioned empirical equation, the knitted FCB should withstand more than 10^7 cycles at 20% maximum strain, consistent with an average extension of the human skin [4] (figure 4*a*). To confirm this, we further conducted a cyclic tensile test for 1 000 000 cycles (equivalent to three months of normal wear) at a set strain of 20%. The electrical resistance remains unchanged ((Rmax−Rmin)/Rmin≈0.65Rmax−Rmin)/Rmin≈0.65%) over 1 000 000 cycles of 20% applied strain in the transverse case, as shown in figure 4*b*, demonstrating the knitted FCB could pass the test without electrical failure. The SEM image (figure 4*c*) taken after 1 000 000 cyclically tensile tests also proves that three-dimensionally looped metal fibres in the knitted FCB are still intact, without any mechanical degradation.

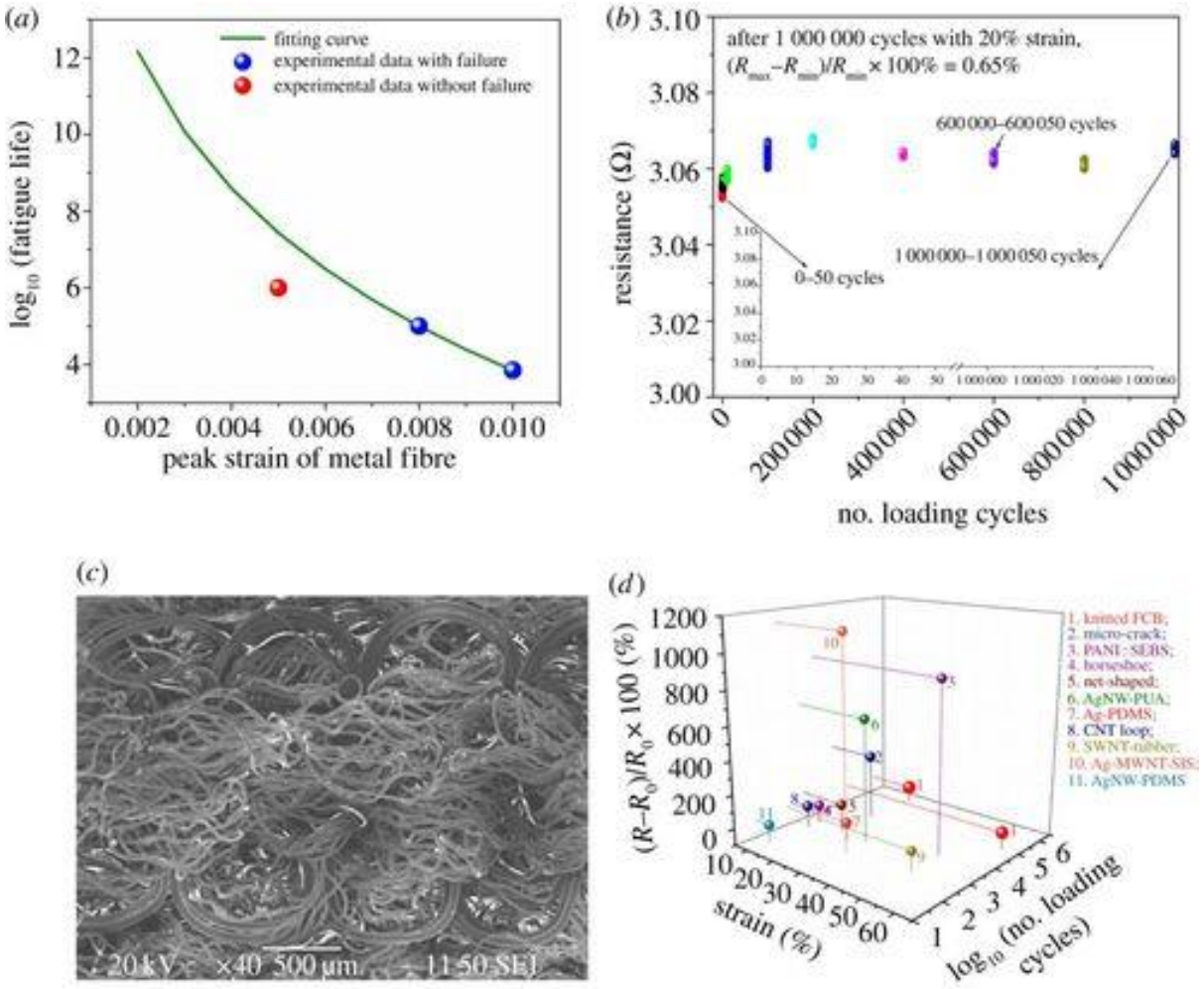

Figure 4. Fatigue life of the knitted FCB. (*a*) The predicted fatigue life with Coffin–Manson law. (*b*) Electrical resistance of the FCB plotted against number of tensile cycles (maximum FCB strain of 20%). (*c*) SEM image of the sample after 1 000 000 cyclical tensile test with 20% maximum FCB strain. (*d*) Comparison with others' published work (2, microcrack [116]; 3, PANI : SEBS [75]; 4, horseshoe [108]; 5, net-shaped [20]; 6, AgNW–PUA [114]; 7, Ag–PDMS [109]; 8, CNT loop [74]; 9, SWNT–rubber [72]; 10, Ag–MWNT-SIS [73]; 11, AgNW–PDMS [111]).

A comparison with others' published work is shown in figure 4*d* [41]. The fatigue life varies from 50 cycles at 10% maximum strain (AgNW in the PDMS substrate [111]) to 25 000 cycles at 20% maximum strain with 300% relative change in electrical resistance (microcracked pattern [116]). The low reported fatigue life with substantial change in electrical resistance may prevent their use as wearable applications. By contrast, the knitted FCB maintains its electrical

resistance almost constant (variation of 0.65%) over exceptionally large loading–unloading cycles of 1 000 000 cycles owing to structural conversion of knitted fabric and mitigation in strain of the metal fibres when they are interlaced with smooth and compliant multi-filament yarns in three-dimensionally looped configurations.

A more critical demand for wearable applications is washing capability in repeated usage. We washed four groups of FCB specimens (length: approx. 10 cm) in a washing machine at 40°C and then dried them at 75°C 30 times according to AATCC standard 135: dimensional changes of fabrics after home laundering (electronic supplementary material, figure S6). We found that electrical failure started to occur at the 10th wash for a specimen without the protection of a mesh bag (thickness: approx. 0.27 mm; electronic supplementary material, figure S6*c*) in 'normal' cycle (agitation speed: 179–119 spm (spm=strokes per minute); spin speed: 645 rpm), in which 84% of specimens (total number: 30) have little or no change in electrical resistance of 5.5 Ω after 30 washing–drying cycles. The resistance retention ratio, which was defined as the ratio of the number of specimens maintaining electrical integrity to the total number of specimens in the washing test, rose to 89% when the specimens were put into a protective mesh bag (figure 5*a*). The SEM observation after 30 washing cycles reveals that no visible fractures can be found on the specimens maintaining electrical integrity, suggesting that the polyurethane coating adheres well to the core metal fibre, so that the presence of water with detergent, mechanical agitation at elevated washing and drying temperature do not damage the metal fibres (electronic supplementary material, figure S6*d*). Electrical failure, on the other hand, was induced by mechanical breakage of the metal fibres (figure 5*b*), because the knitted FCBs were subjected to strong mechanical actions causing deformation, including stretching, bending, compression and rubbing in the washing process. Hence, the resistance retention ratio is much better using the 'delicates' cycle with reduced mechanical agitation (agitation speed: 119 spm; spin speed: 430 rpm), where all 60 specimens passed the 30 washing test cycles without any apparent electrical degradation (figure 5*a*).

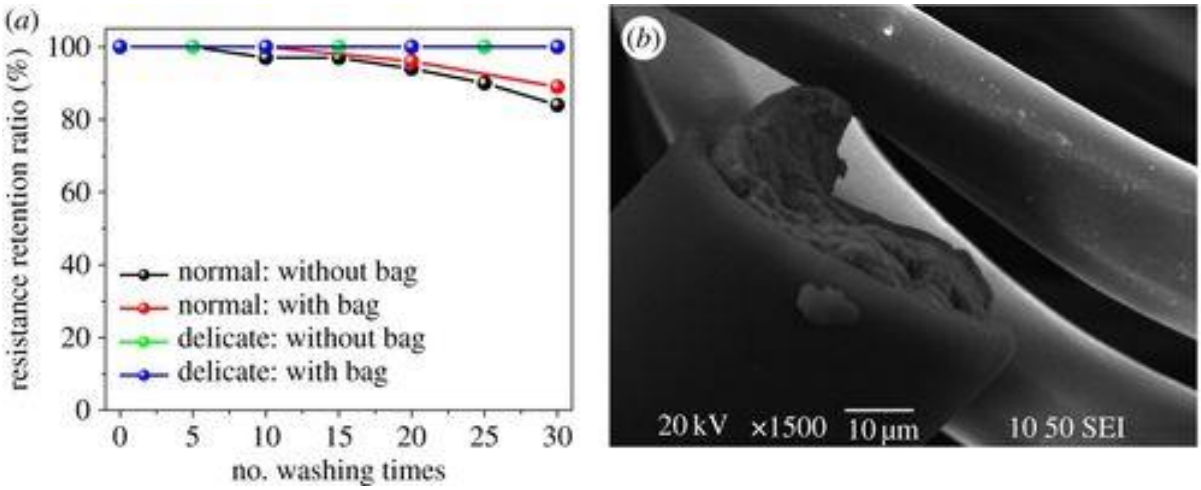

Figure 5. Washing capability of the knitted FCB. (*a*) Resistance retention ratio in the washing tests. (*b*) SEM image of one failed metal fibre in the knitted FCB after 30 times in 'normal' washing cycle.

In wearable electronic applications, strain distribution of the conductive tracks plays an indispensable role in determination of deformability, relative resistance change and fatigue life [117]. We expect that local strain of the metal fibres in the knitted FCB is mitigated through the loop configuration in the knitted fabric composed of compliant and smooth multifilament yarns, which represent a very soft dielectric element to support the metal fibres at their contact regions. To reveal the underlying mechanism, we analysed the three-dimensionally knitted loops, based on Leaf's model [118], assuming that the metal fibre is a thin elastic rod [119]. Such a knitted loop is shown in figure 6*a*, depicting that the initial straight metal fibre has deformation simultaneously in two planes at an angle to one another; the curvature k and torsion τ of the fibre axis are given by $k = \sqrt{x''^2 + y''^2 + z''^2}$ and

$$\tau = \begin{vmatrix} x' & y' & z' \\ x'' & y'' & z'' \\ x''' & y''' & z''' \end{vmatrix} / k^2,$$

respectively, where x, y and z represents the coordinates of an arbitrary point on the metal fibre, and the dashes denote differentiation with respect to the arc length (figure 6*b*, where $0 \leq \phi \leq \pi/2$,

see the electronic supplementary material). The derived geometry from Leaf's model coincides with SEM observations in the initial state (figure 1), i.e. the metal fibre is primarily bent (at the circular portion) and secondarily twisted (at the straight segment) into a three-dimensionally looped configuration. Hence, induced bending (ε_b) and shear (γ_s) strain of the metal fibre at the loop formation is $\varepsilon_{b\max}=d_{fibre}k/2$ and $\gamma_{s\max}=d_{fibre}\tau/2$, respectively, where d_{fibre} is the fibre diameter. The local strain of the metal fibre, represented by equivalent Von Mises strain, could then be obtained from $\varepsilon_{eq}=2/3\sqrt{3/2\varepsilon_{b\max}^2+3/4\gamma_{s\max}^2}$. Figure 6*c*,*d* plots bending and shear strain of the metal fibre in the three-dimensionally looped configuration, such that (i) peak bending strain occurs at the crest and trough of the loop, corresponding to maximum curvature; (ii) peak shear strain is induced from the circular portion to the straight segment of the loop, corresponding to maximum torsion; (ii) both fibre diameter and loop length affect local strain of the metal fibre in the loop. Thus, it is of great importance to determine the unit loop length, before incorporation of a metal fibre with a predefined diameter into a knitted loop, in order to achieve satisfactory mechanical and electrical integrity (electronic supplementary material, figure S3*b*).

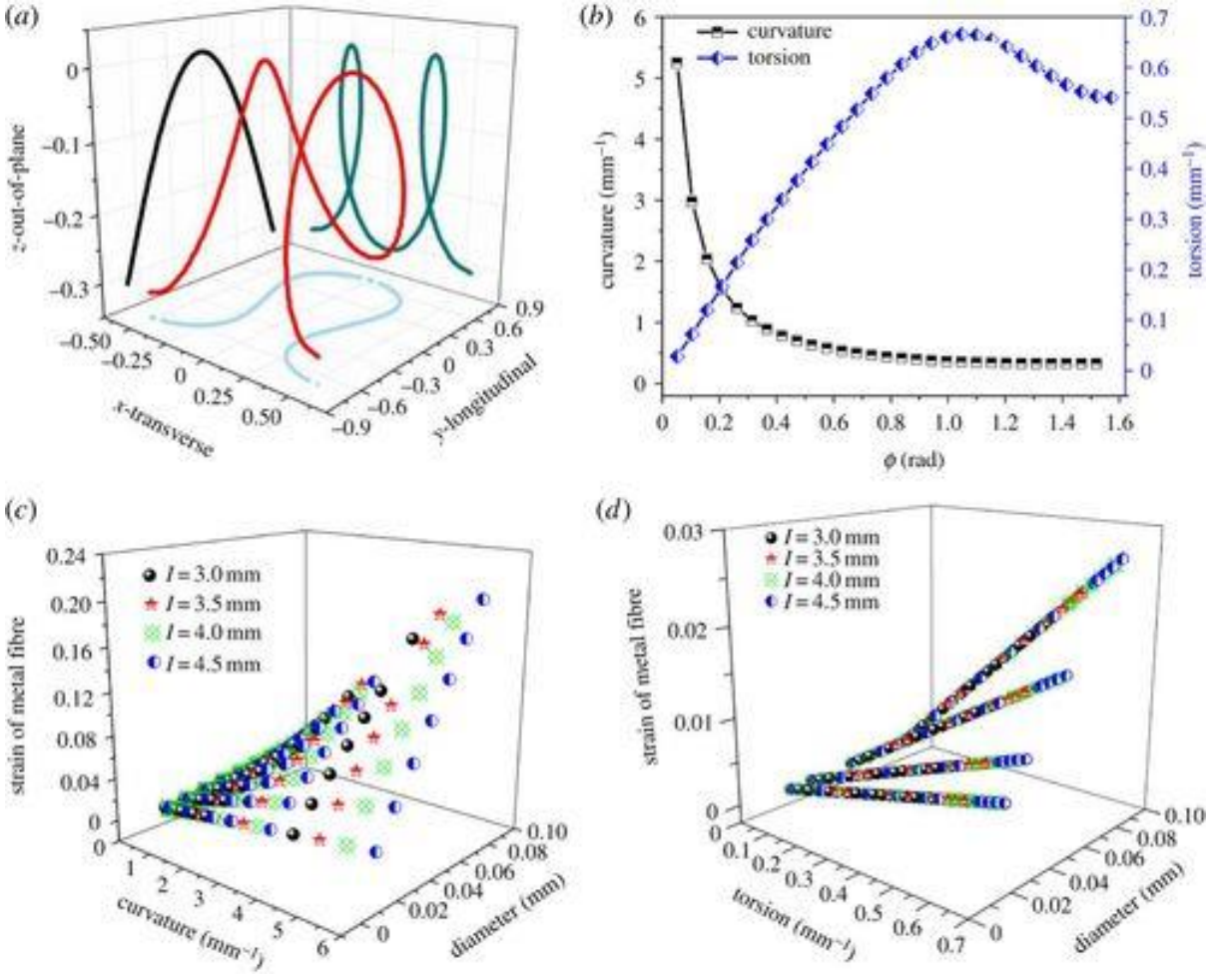

Figure 6. Geometrical configuration and fibre strain at the loop formation. (*a*) Three-dimensionally looped configuration. (*b*) Corresponding curvature and torsion. (*c*) Fibre bending strain plotted against curvature and fibre diameter. (*d*) Fibre shear strain plotted against torsion and fibre diameter.

To derive the peak strain of the metal fibres when the knitted FCB was subjected to an applied strain, three-dimensional finite-element simulation was conducted (electronic supplementary material, figure S7). Peak strain of both free-standing and interlaced metal fibres is plotted in figure 7*a*, with applied FCB elongation in the transverse and longitudinal directions, respectively. Within the simulation range, the peak strain of free-standing and interlaced metal fibre loops are the same until FCB elongation reaches a threshold value of 21% in the longitudinal tensile test, implying that the metal fibres are free to deform in the FCB. This threshold value is much lower, i.e. 12% in the transverse tensile test. The physical meaning of this value can be interpreted as 'when the metal fibre is transferred from a free-standing looped state to an interlaced state with a filament yarn, its deformation is limited by contact friction and pressure'. Moreover, peak strain of the metal fibre remained the same as before the threshold values, indicating that a loose-knitted structure mitigates peak strain of the rigid metal fibre in the soft- and porous-knitted fabric, therefore enhancing mechanical and electrical integrity of the FCB. Figure 7*b–e* depicts the influence of three factors, i.e. unit loop length, ratio of elastic moduli as well as ratio of diameters, on the peak strain of the metal fibre interlaced with a filament yarn. The peak strain of the metal fibre can be further reduced through ways of increasing its unit loop length (figure 7*b*), lowering Young's modulus of the interlacing filament yarn ($E_{yarn}/E_{metal}\approx0.0001$; figure 7*c*) as well as reduction in the diameter of the filament yarn ($diameter_{yarn}/diameter_{metal}\approx0.5$, figure 7*d–e*) in both transverse and longitudinal directions. The results of numerical simulation are consistent with experimental observations on geometrical changes of the metal fibres in the knitted FCB (electronic supplementary material, figure S7).

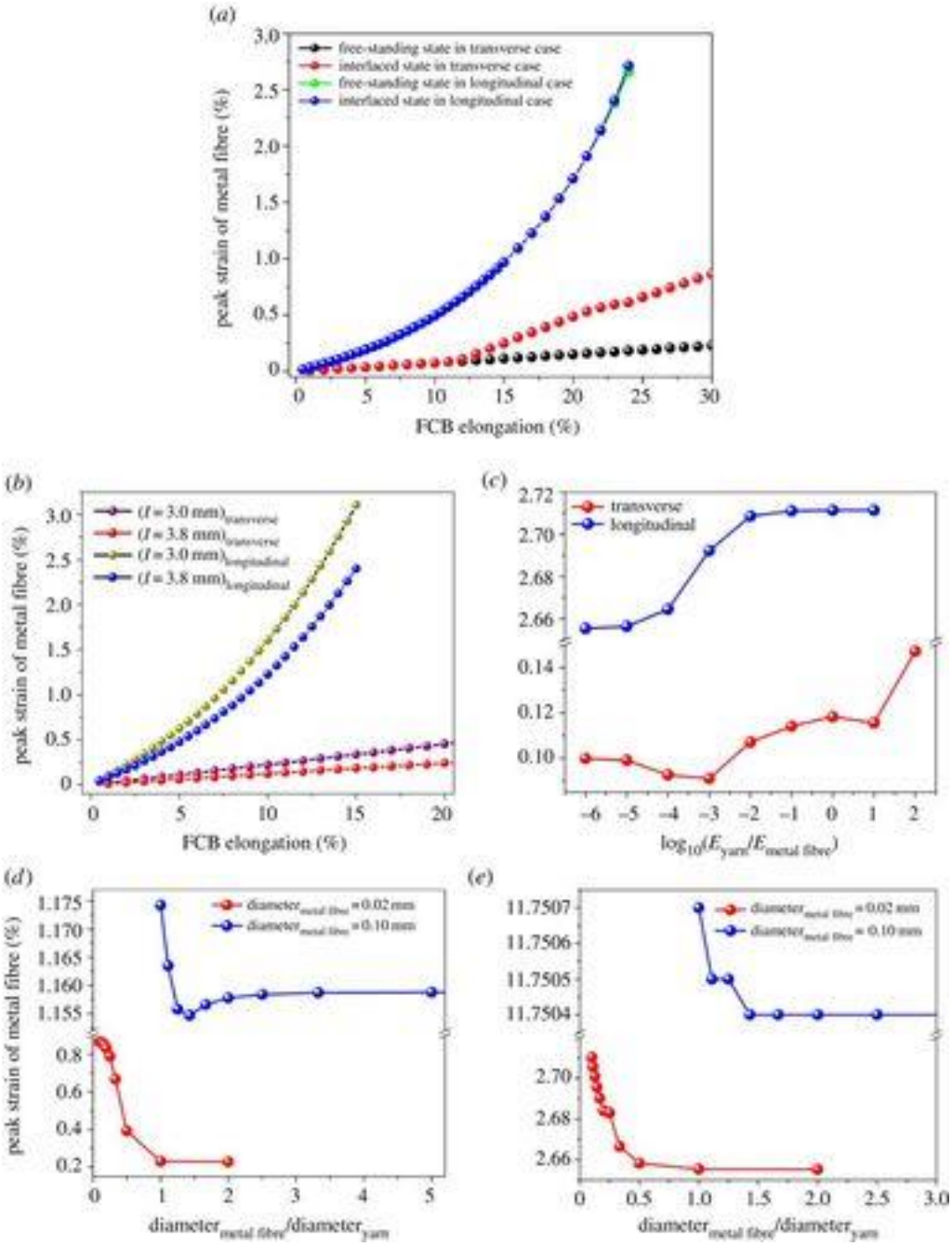

Figure 7. Peak strain of metal fibre when the knitted FCB was elongated. (*a*) Peak strain of the metal fibre from a free-standing state to an interlaced state. (*b*) Effects of unit loop length. (*c*) Effects of ratio of Young's moduli. (*d*,*e*) Effects of ratio of fibre diameters in the transverse and longitudinal directions, respectively.

3. Application

To the best of our knowledge, the performance of the present knitted FCBs has far exceeded those of previously reported metal-coated elastomeric films or other organic materials in terms of changes in electrical resistance, three-dimensional deformability, fatigue life and washing capability as well as permeability [120,121]. Those distinctive features make the knitted FCBs particularly suitable for next-to-skin electronic devices. As a demonstration, we have fabricated a flexible and stretchable fabric sensing network as a knitted FCB assembly to be used for *in situ* measurement of strain and deformation of a smart bulletproof vest.

In the knitted FCB assembly, discrete strain sensor elements (Softceptor, from AdvanPro Limited, Hong Kong) on different locations were mechanically and electrically connected by conductive tracks of the FCB. The resistive sensor element (initial resistance: approx. 6.68 (±0.71) kΩ with a dimension of 5×10×0.5 mm) with two soft polymeric electrodes could measure strain up to 60% with different strain rates (from 0.05 to 1000 s^{-1}) [122]. Figure 8*a* presents a fabrication sequence for the fabric sensing network, composed of eight sensor elements in an exampled 'eight diagram' pattern, which was designed for *in situ* measurement of strain during ballistic impact, therefore opening up potential applications as smart protective apparel. The first step involves knitting an intarsia pattern on the computerized knitting machine (electronic supplementary material, figure S4*b*) to define wiring layout of the FCB corresponding to predetermined locations of the eight independent sensor elements. The minimum distance between two adjacent conductive 'tracks' in the FCB could reach approximately 1 mm and the largest 'track' length, in the transverse direction of the FCB, could reach approximately 2140 mm with the current computerized flat-bed knitting machine. The fabric dimensions were determined by experiments. The thickness was estimated by filament yarn diameter (approx. 800 μm), without the influence of extension and bending [123]. In the next step, eight sensor elements with two parallel soft electrodes (distance: 10 mm) were placed (adhered or sewn) on corresponding locations of the undeformed knitted FCB in a precision fashion, because the FCB was first fixed on a rigid platform. Third, the sensor electrodes went through the 'vias' (micropores of the knitted FCB) using a rigid needle (diameter: approx. 0.6 mm) and were physically linked by the looped metal fibres through novel 'helical connections' for transmission of electrical signals to outer circuits (figure 8*b* and electronic supplementary material, figure S8). Here, a helical geometry and subsequent semi-spherical compliant encapsulation, 'helical connection' for short, was for the first time

proposed to enhance mechanical robustness [124] and prevent damage of the whole assembly as well as electrical shorting from surrounding environments [90] between the sensor electrodes and the metal fibre loops. The induced contact resistance was neglectable and constant ($(R-R_0)/R_0\times100(\%)<0.5\%$) with applied strain in tensile and three-dimensional punch tests owing to geometrical adjustments of the helix in its in-plane radius, pitch and angle (figure 8*c* and electronic supplementary material, figure S9). The final step was to connect the other ends of the conductive tracks in the knitted FCB to outer circuits by means of bonding selected interposers to the metal fibre loops with a compliant silicone adhesive and then stiffening the connected region with a thin layer of woven fabric with a maximum mechanical strain of less than 20%. After fabrication, the electrical resistance of one sensor element was monitored when it was unidirectionally stretched. The two curves in the electronic supplementary material, figure S10, represent the relationships between the relative change in electrical resistance and strain of the sensor element before and after fabrication, exactly overlapped with each other, demonstrating that the electromechanical behaviour of the sensor element was not affected by the fabrication process, the knitted fabric (with a modulus: less than 1 MPa), as well as looped metal fibres and helical connections. The described FCB fabrication technology is well compatible with the existing 'island-bridge' approach [90,125] to fabrication methods of all the flexible and stretchable devices.

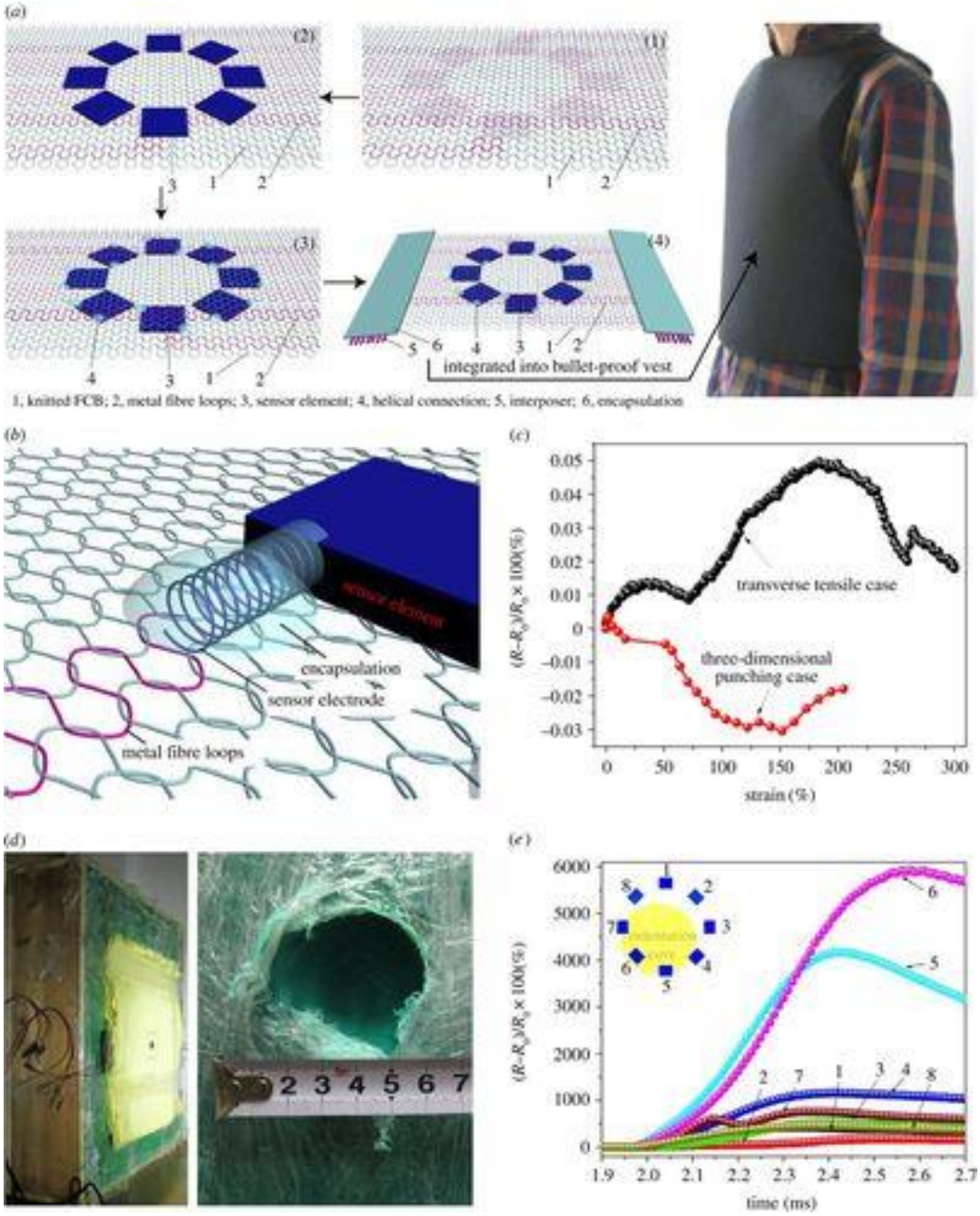

Figure 8. Fabrication and application of a fabric sensing network integrated into a bulletproof vest. (*a*) Fabrication procedures of the fabric sensing network integrated into a bulletproof vest. (*b*) Helical connection from the sensor electrode to conductive track of the knitted FCB. (*c*) Relative resistance change of the helical connection as functions of tensile and punching strains. (*d*) Fabric sensing network integrated into kevlar fabrics for *in situ* ballistic impact measurement. (*e*) Relative resistance change of the sensor elements measured during a ballistic impact.

The packaged fabric sensing network was then inserted between multi-plies of energy absorbing fabrics (Kevlar or UHMWPE) for smart bulletproof vests (figure 8*a*). To test the ballistic performance of the vest, the multi-plies with fabric sensing network was placed on a soft foundation material (clay or gelatin). Then, a bullet was fired with various speeds at the centre of the sensing network and *in situ* strain measurement by the sensor network was conducted during ballistic impact (figure 8*d* and the electronic supplementary material, table S2). The indentation cave produced on the clay had a diameter of 51(±9.1) mm and depth of 18(±6.8) mm, implying that the fabric sensing network was three-dimensionally deformed with a large strain during the impact. Figure 8*e* shows that the sensors closer to the impact point underwent larger strains with earlier onset of resistance change as a result of elastic strain wave propagated from the impact point to surrounding regions, and the kinetic energy of the bullet was dissipated by the energy absorbing fabrics in the propagation process. Hence, the bullet was stopped. The knitted FCBs have shown excellent reliability during the ballistic impact tests as all 35 sensor network assembly samples performed well without mechanical and electrical failure and received reliable electrical signals. The details of this work will be reported separately in the near future.

4. Conclusion

In this paper, we have reported the design, fabrication and characterization of three-dimensionally deformable, durable and washable knitted FCBs made by interlacing coated metal fibres with elastic multi-filament yarns using computerized knitting technologies. The resultant knitted FCBs exhibit outstanding electrical stability with a large strain (less than 1% relative resistance change within 300% tensile strain), extraordinary fatigue life (greater than 1 000 000 cycles at 20% maximum strain) and satisfactory washing capability (30 times with ‘delicates’ washing cycle). In combination, the knitted FCBs offer the best performance for wearable electronic applications when compared with previously reported elastomer films. Theoretical analysis and numerical simulation show that structural conversion of knitted fabrics is attributed to the effective mitigation of strain of the metal fibres. The knitted FCB structures permit easy adjustment of their geometrical configurations of the metal fibre loops (i.e. period and amplitude); in addition, they permit free slippage and transfer of the loops that are subjected to very low friction and compression from compliant and smooth interlacing multifilament yarns. We have further demonstrated the feasibility of application of the knitted FCBs in smart protective apparel for *in situ* measurement during ballistic impact.

Knitted FCBs have great potential in a wide range of applications, such as human/electronic interfaces, skin-mounted systems, as well as next-to-skin monitoring systems for healthcare, because the knitted FCB possesses high three-dimensional deformability, low tensile, shear and bending rigidities, and excellent breathability and durability for long-term use. In addition, the knitted FCB technologies have some similarity to and advantages over main-stream flexible printed circuit boards in terms of the computer-aided structural design and green cost–effect manufacture. First, the knitted FCBs allow patterning electronic building blocks on either the front side or back side or on multi-layers owing to 'vias' in the form of inherent micropores, which enable conductive fibres or leads to pass through the FCB, thereby providing more diversity, such as three-dimensional heterogeneous schemes in the placement of sophisticated electronic components. Second, the full computer-integrated manufacturing capacity directly facilitates mass production of medium- to large-area knitted FCBs with precise geometrical layouts with a spatial resolution of approximately 1 mm in a reliable and inexpensive manner. All operations are at ambient dry conditions, no chemicals are used or discharged in the manufacturing processes at all. Therefore, the combination of outstanding performance of the knitted FCBs and well-established manufacturing technologies with CAD and SIM will lead to a bright future in the development of wearable electronics.

5. Experimental set-up

(a) Structure of fabric circuit board

A variety of knitted fabrics, composed of interlaced yarns in a series of connected loops, has been considered for FCBs because they can be produced with modern precision machinery that possess full computer-aided design and integration manufacturing capacity. A single jersey-knitted structure was chosen for FCBs in this study owing to its superior resilience and relatively isotropic extensibility in transverse and longitudinal directions as well as acceptable thickness (approx. 2*d*, where *d* is the yarn diameter) as inner garments for comfort compared with other knitted structures, such as rib, interlock and purl as well as warp knitted ones (electronic supplementary material, figure S2) [126].

(b) Materials for conductive tracks

Three types of conductive fibres have been investigated for previous textile-based electrical wirings, i.e. pure metal fibres, intrinsically conductive polymers and metal-plated fibres [30,127]. Commercial copper continuous fibres of core diameter of 50 μm, coated by

polyurethane with a thickness of 3 μm, were obtained from Shanghai Gold Fine Enameled Wire Co., Ltd, China. The fine metal fibres were chosen as conductive tracks for knitted FCBs owing to their superior conductivity (the resistivity of copper fibre with 20 μm core diameter is approx. 0.55 $\Omega\,\mathrm{cm}^{-1}$) and current carrying capacity of 15 mA, satisfying standard IPC-9252A: the requirements for electrical testing of unpopulated printed boards.

(c) Dielectric supporting materials

We selected textured multi-filament yarns made from polyamide fibres by considering the following: (i) soft and flexible textile materials used for intimate apparel; (ii) good dielectric constant and little moisture regain; (iii) appropriate thermal and chemical stability; (iv) smooth surface that enables less friction allowing the metal fibres to have more freedom to slide and transfer among the loops, hence accommodating a large level of mechanical FCB strain; and (v) low materials and manufacturing costs (electronic supplementary material, table S1) [128]. We also selected spandex filament yarns because of their super extensibility and elasticity (up to 400–800% strain [129] and recovery of almost 100% from 400% strain) attributed to hard and soft segments in its molecular structure [126]. The spandex filament yarns are incorporated with a pre-tension of approximately 1 cN (corresponding pre-strain of 150%) into the loop structure to make the knitted FCBs more stretchable and capable of returning to their original dimensions, hence imparting better fitting [126,129]. Textured multi-filament yarns, i.e. a highly elastic spandex filament yarn in the core (Dupont Lycra, 20dtex/2f) and polyamide multifilaments wrapped around the core (70dtex/24f), were obtained from Sun Hing, Hong Kong (electronic supplementary material, figure S3*c*).

(d) Fabrication methods

A circuit diagram was first designed with consideration of all electronic components and data ports. The working frequency and current carry capacity were also taken into account. Different from the weaving technology which limits the wiring layout in transverse (welf) and longitudinal (warp) directions, it is feasible to 'knit'-stretchable FCBs with a complicated geometrical layout such as array, matrix, network and any arbitrary configurations with computerized knitting technology (electronic supplementary material, figure S4*a*,*b*). The intarsia pattern in single jersey-knitted fabrics was selected for the FCB when the stitch density and dimensions were decided by experiments beforehand. An intarsia knitting chart was constructed based on a computer program which was written to drive a computerized flat-bed

knitting machine (STOLL CMS822, gauge: 14). Two copper fibres were fed into the knitting machine with a minimum tension together with the filament yarns at tension of approximately 1 cN, corresponding to approximately 150% pre-strain.

(e) Characterization

Optical microscopy observation was performed on a Leica M165C (DFC 290HD, Leica Microsystems Ltd., Hong Kong). SEM observation of the FCB samples from 0% to 60%, and to 120% strain in the transverse and longitudinal directions was conducted on a field emission scanning electron microscope (JEOL JSM-6335F, JEOL Ltd., Japan). The relative resistance change of the knitted FCBs with applied strain was investigated under different deformation modes. The unidirectional tensile tests were performed on an Instron Universal Material Tester, where the sample (2.5×7 cm) was fixed to the top and bottom clamps with gauge length of 5 cm. The tensile speed was 300 mm min^{-1}. Ball punching measurement was conducted on an Instron Universal Material Tester with a ball–burst attachment, consisting of a ring clamp (diameter: approx. 44.45 mm) to hold the test specimen with the metal fibre lines in the centre and a polished stainless steel ball (diameter: approx. 25.4 mm) attached to the movable member of the tensile tester. The ball was punched into the FCBs with a cross-head speed of 300 mm min^{-1}. The conductive tracks in the knitted FCB were connected to a high-precision digital multimeter (Keithley 2010, Keithley Instruments Inc. USA) interfaced with a personal computer. The electrical resistance was monitored when the samples were stretched unidirectionally and punched three-dimensionally to failure either electrically or mechanically. For the fatigue test, each cycle corresponded to the deformation to a certain level of maximum strain (i.e. 20%, 60% and 80%) and then returned to the original state with a tensile speed of 500 mm min^{-1}.

(f) Washability

The washing test was conducted on a vertical-axis washing machine (Whirlpool, USA) referring to AATCC standard 135: dimensional changes of fabrics after home laundering. The knitted FCBs (length: approx. 15 cm) together with ballast (total load: 1.8 kg), with a commercial non-ionic detergent (Castle super concentrate with double lemon fragrance, 66 g), was washed at approximately 40°C with ‘normal’ (agitation speed: from 179 to 119 spm; spin speed: 645 rpm, rpm=revolutions per minute) or ‘delicates’ (agitation speed: 119 spm; spin speed: 430 rpm) cycles and the knitted FCBs were then dried under 75°C with ‘automatic dry’

cycle. The whole procedure was conducted 30 consecutive times with four groups: (i) original FCB samples with ‘normal’ cycle; (ii) FCB samples in a mesh bag with ‘normal’ cycle; (iii) original FCB samples with ‘delicates’ cycle; and (iv) FCB samples in a mesh bag with ‘delicates’ cycle. The electrical resistance was monitored after each drying treatment during the cyclic washing tests.

(g) Finite-element simulations

The simulation was conducted by using the structural mechanics module of ANSYS 13.0. Half of a unit cell was investigated, owing to geometrical symmetry, consisting of a three-dimensionally looped metal fibre (element type: Beam188, diameter: 20 μm; elastic modulus: 115 GPa, Poisson's ratio: 0.32) interlaced with a filament yarn (element type: beam 188, diameter: 200 μm, elastic modulus: 2.8 GPa, Poisson's ratio: 0.37), with applied FCB elongation in the transverse and longitudinal directions, respectively. The contact model was built up by a three-dimensional line to line contact (electronic supplementary material, figure S7). Loops in free standing status and in contact mode with interlacing yarns were considered when applying unidirectional elongations in the transverse and longitudinal directions of the knitted FCB.

Acknowledgements

Li Qiao thanks the Hong Kong Polytechnic University for a postgraduate scholarship. Authors also acknowledge Ms Liu Su for technical support for knitting of the FCB samples; Dr Zhu Bo, Mr Wen Xiaojian and Chen Song, Ms Wang Yanming for supports in the ballistic impact experiments. Both authors contributed equally to this work.

Funding statement

The authors acknowledge funding support from Research Grants Council of the Hong Kong SAR Government, National Science Foundation of China (grant no. PolyU503/12, PolyU5251/13, PolyU152152/14E), Hong Kong Research Institute of Textile and Apparel (grant no. ITP/007/10TP) for this research; and Nanjing University of Science and Technology for providing technical support for the ballistic experiments.

References

1. Zeng W, Tao XM, Chen S, Shang SM, Chan HLW, Choy SH. 2013 Highly durable all-fiber nanogenerator for mechanical energy harvesting.Energy Environ. Sci.6, 2631–2638.(doi:10.1039/C3ee41063c)

2. Cherenack K, Zysset C, Kinkeldei T, Munzenrieder N, Troster G. 2010 Woven electronicfibers with sensing and display functions for smart textiles.Adv. Mater.22, 5178–5182.(doi:10.1002/adma.201002159)

3. Wang F, Zhu B, Shu L, Tao XM. 2014 Flexible pressure sensors for smart protectiveclothing against impact loading.Smart Mater. Struct.23, 015001. (doi:10.1088/0964-1726/23/1/015001)

4. Yamada T, Hayamizu Y, Yamamoto Y, Yomogida Y, Izadi-Najafabadi A, Futaba DN, HataK. 2011 A stretchable carbon nanotube strain sensor for human-motion detection.Nat.Nanotechnol.6, 296–301. (doi:10.1038/Nnano.2011.36)

5. Salvatore GA, Munzenrieder N, Kinkeldei T, Petti L, Zysset C, Strebel I, Buthe L, Troster G.2014 Wafer-scale design of lightweight and transparent electronics that wraps around hairs.Nat. Commun. 5, 2982. (doi:10.1038/Ncomms3982)

6. Petti L, Munzenrieder N, Salvatore GA, Zysset C, Kinkeldei T, Buthe L, Troster G. 2014Influence of mechanical bending on flexible InGaZnO-based ferroelectric memory TFTs.IEEE Trans. Electron. Dev.61, 1085–1092. (doi:10.1109/Ted.2014.2304307)

7. Xu Set al. 2014 Soft microfluidic assemblies of sensors, circuits, and radios for the skin.Science344, 70–74. (doi:10.1126/science.1250169)

8. Fan JAet al. 2014 Fractal design concepts for stretchable electronics.Nat. Commun.5, 1–8.(doi:10.1038/Ncomms4266)

9. Kim DHet al. 2012 Electronic sensor and actuator webs for large-area complex geometrycardiac mapping and therapy.Proc. Natl Acad. Sci. USA109, 19 910–19 915. (doi:10.1073/pnas.1205923109)

10. Tao XM. 2005Wearable electronics and photonics, 250 S. p. Boca Raton, FL: CRC Press.

11. Someya T. 2013Stretchable electronics, 462 pp. Weinheim, Germany: Wiley-VCH.

12. Coyle Set al. 2010 BIOTEX-biosensing textiles for personalised healthcare management.IEEETrans. Inf. Technol. Biomed.14, 364–370. (doi:10.1109/Titb.2009.2038484)

13. Kannaian T, Neelaveni R, Thilagavathi G. 2013 Design and development of embroideredtextile electrodes for continuous measurement of electrocardiogram signals.J. Ind. Text.42,303–318. (doi:10.1177/1528083712438069)

14. Scilingo EP, Lorussi F, Mazzoldi A, De Rossi D. 2003 Strain-sensing fabrics for wearablekinaesthetic-like systems.IEEE Sens. J.3, 460–467. (doi:10.1109/Jsen.2003.815771)
15. Holleczek T, Ruegg A, Harms H, Troster G. 2010 Textile pressure sensors for sportsapplications. InSensors, 2010 IEEE, Kona HI, 1–4 November, pp. 732–737. New York, NY: IEEE.(doi:10.1109/Icsens.2010.5690041)
16. Raskovic D, Martin T, Jovanov E. 2004 Medical monitoring applications for wearablecomputing.Comput. J.47, 495–504. (doi:10.1093/comjnl/47.4.495)
17. Menon Cet al. 2009 Prospects of brain–machine interfaces for space system control.ActaAstronaut.64, 448–456. (doi:10.1016/j.actaastro.2008.09.008)
18. Kaltenbrunner Met al. 2013 An ultra-lightweight design for imperceptible plastic electronics.Nature499, 458–463. (doi:10.1038/Nature12314)
19. Someya T, Sekitani T, Iba S, Kato Y, Kawaguchi H, Sakurai T. 2004 A large-area, flexiblepressure sensor matrix with organic field-effect transistors for artificial skin applications.Proc. Natl Acad. Sci. USA101, 9966–9970. (doi:10.1073/pnas.0401918101)
20. Someya T, Kato Y, Sekitani T, Iba S, Noguchi Y, Murase Y, Kawaguchi H, Sakurai T. 2005Conformable, flexible, large-area networks of pressure and thermal sensors with organictransistor active matrixes.Proc. Natl Acad. Sci. USA102, 12 321–12 325. (doi:10.1073/pnas.0502392102)
21. Rogers JA, Someya T, Huang YG. 2010 Materials and mechanics for stretchable electronics.Science327, 1603–1607. (doi:10.1126/science.1182383)
22. Lumelsky VJ, Shur MS, Wagner S. 2001 Sensitive skin.IEEE Sens. J.1, 41–51. (doi:10.1109/Jsen.2001.923586)
23. Zysset Cet al. 2013 Textile integrated sensors and actuators for near-infrared spectroscopy.Opt. Express.21, 3213–3224. (doi:10.1364/OE.21.003213)
24. Bian ZG, Song JZ, Webb RC, Bonifas AP, Rogers JA, Huang YG. 2014 Thermal analysis ofultrathin, compliant sensors for characterization of the human skin.RSC Adv.4, 5694–5697.(doi:10.1039/C3ra45277h)
25. Kim DH, Lu NS, Huang YG, Rogers JA. 2012 Materials for stretchable electronics inbioinspired and biointegrated devices.MRS Bull.37, 226–235. (doi:10.1557/Mrs.2012.36)
26. Kim DHet al. 2008 Complementary metal oxide silicon integrated circuits incorporatingmonolithically integrated stretchable wavy interconnects.Appl. Phys. Lett.93, 044102.(doi:10.1063/1.2963364)
27. Kim DHet al. 2009 Optimized structural designs for stretchable silicon integrated circuits.Small5, 2841–2847. (doi:10.1002/smll.200900853)

28. Shen J, Chui CH, Tao XM. 2013 Luminous fabric devices for wearable low-level light therapy.Biomed. Opt. Express.4, 2925–2937. (doi:10.1364/Boe.4.002925)
29. Shu L, Hua T, Wang YY, Li QA, Feng DD, Tao XM. 2010 In-shoe plantar pressuremeasurement and analysis system based on fabric pressure sensing array.IEEE Trans. Inf.Technol. B14, 767–775. (doi:10.1109/Titb.2009.2038904)
30. Cottet D, Grzyb J, Kirstein T, Troster G. 2003 Electrical characterization of textile transmissionlines.IEEE Trans. Adv. Packag.26, 182–190. (doi:10.1109/Tadvp.2003.817329)
31. Locher I, Troster G. 2008 Enabling technologies for electrical circuits on a wovenmonofilament hybrid fabric.Text. Res. J.78, 583–594. (doi:10.1177/0040517507081314)
32. Chedid M, Belov I, Leisner P. 2007 Experimental analysis and modelling of textiletransmission line for wearable applications.Int. J. Cloth. Sci. Technol.19, 59–71. (doi:10.1108/09556220710717053)
33. Mattila HR. 2006Intelligent textiles and clothing, 506 S. p. Boca Raton, FL: CRC Press.
34. Dhawan A, Seyam AM, Ghosh TK, Muth JF. 2004 Woven fabric-based electricalcircuits. Part I: evaluating interconnect methods.Text. Res. J.74, 913–919. (doi:10.1177/004051750407401011)
35. Dhawan A, Ghosh TK, Seyam AM, Muth JF. 2004 Woven fabric-based electrical circuits. II.Yarn and fabric structures to reduce crosstalk noise in woven fabric-based circuits.Text. Res.J.74, 955–960. (doi:10.1177/004051750407401103)
36. Li Q, Tao XM. 2011 A stretchable knitted interconnect for three-dimensional curvilinearsurfaces.Text. Res. J.81, 1171–1182. (doi:10.1177/0040517511399965)
37. Dunne LE, Bibeau K, Mulligan L, Frith A, Simon C. 2012 Multi-layer e-textile circuits. InProc. 2012 ACM Conf. on Ubiquitous Computing, Pittsburgh, PA, 5–8 September, pp. 649–650.New York, NY: ACM.
38. Katragadda RB, Xu Y. 2007 A novel intelligent textile technology based on silicon flexibleskins. InProc. IEEE Twentieth Annual Int. Conf. on Micro Electro Mechanical Systems, Hyogo,Japan, 21–25 January, vols 1 and 2, pp. 55–58. New York, NY: IEEE.
39. Post ER, Orth M, Russo PR, Gershenfeld N. 2000 E-broidery: design and fabrication of textile-based computing.IBM Syst. J.39, 840–860. (doi:10.1147/sj.393.0840)
40. Linz T, von Krshiwoblozki M, Walter H, Foerster P. 2012 Contacting electronics to fabriccircuits with nonconductive adhesive bonding.J.Text.Inst.103, 1139–1150. (doi:10.1080/00405000.2012.664867)

41. Zhang H, Tao XM, Yu TX, Wang SY. 2006 Conductive knitted fabric as large-straingauge under high temperature.Sens. Actuators A, Phys.126, 129–140. (doi:10.1016/j.sna.2005.10.026)

42. Yang Y, Cho G. 2009 Novel stretchable textile-based transmission bands: electricalperformance and appearance after abrasion/laundering, and wearability.Human–ComputerInteract. Pt III5612, 806–813.

43. Cherenack K, van Pieterson L. 2012 Smart textiles: challenges and opportunities.J. Appl. Phys.112, 091301. (doi:10.1063/1.4742728)

44. Winterhalter CA, Teverovsky J, Wilson P, Slade J, Horowitz W, Tierney E, Sharma V. 2005Development of electronic textiles to support networks, communications, and medicalapplications in future US military protective clothing systems.IEEE Trans. Inf. Technol.Biomed.9, 402–406. (doi:10.1109/Titb.2005.854508)

45. Simon EP, Kallmayer C, Schneider-Ramelow M, Lang KD. 2012 Development of a multi-terminal crimp package for smart textile integration. In2012 4th Electronic System-IntegrationTechnology Conf.(Estc), Amsterdam, The Netherlands, 17–20 September. New York, NY: IEEE.

46. Cherenack KH, Kinkeldei T, Zysset C, Troster G. 2010 Woven thin-film metal interconnects.IEEE Electron Device Lett.31, 740–742. (doi:10.1109/Led.2010.2048993).

47. Ferro M, Pioggia G, Tognetti A, Carbonaro N, De Rossi D. 2009 A sensing seat for humanauthentication.IEEE Trans. Inf. Forensics Sec.4, 451–459. (doi:10.1109/Tifs.2009.2019156).

48. Tada Y, Inoue M, Tokumaru T. 2014 An evaluation of the characteristics of a stretchable inkwire suitable for the measurement of biological signals.J. Text. Inst.105, 692–700. (doi:10.1080/00405000.2013.844419)

49. Paul G, Torah R, Yang K, Beeby S, Tudor J. 2014 An investigation into the durability ofscreen-printed conductive tracks on textiles.Meas. Sci. Technol.25, 025006:025001–025011.(doi:10.1088/0957-0233/25/2/025006)

50. De Rossi D, Carpi F, Lorussi F, Scilingo EP, Tognetti A. 2009 Wearable kinesthetic systems andemerging technologies in actuation for upperlimb neurorehabilitation. In2009 Annual Int.Conf. of the IEEE Engineering in Medicine and Biology Society, Minneapolis, MN, 3–6 September,vols 1–20, pp. 6830–6833. New York, NY: IEEE.

51. Vanello Net al. 2008 Sensing glove for brain studies: design and assessment of itscompatibility for fMRI with a robust test.IEEE/ASME Trans. Mechatron.13, 345–354.(doi:10.1109/TMECH.2008.924115)

52. Giorgino T, Tormene P, Lorussi F, De Rossi D, Quaglini S. 2009 Sensor evaluation for wearablestrain gauges in neurological rehabilitation.IEEE Trans. Neural Syst. Rehabil. Eng.17, 409–415.(doi:10.1109/Tnsre.2009.2019584)

53. Coyle S, Wu YZ, Lau KT, De Rossi D, Wallace G, Diamond D. 2007 Smart nanotextiles:a review of materials and applications.MRS Bull.32, 434–442. (doi:10.1557/Mrs2007.67).

54. Tognetti A, Lorussi F, Tesconi M, De Rossi D. 2004 Strain sensing fabric characterization. InProc. IEEE Sensors 2004, Vienna, Austria, 24–27 October, vols 1–3, pp. 527–530. New York, NY:IEEE.

55. Lorussi F, Scilingo EP, Tesconi M, Tognetti A, De Rossi D. 2005 Strain sensing fabric for handposture and gesture monitoring.IEEE Trans. Inf. Technol. Biomed.9, 372–381. (doi:10.1109/Titb.2005.854510).

56. Tesconi M, Scilingo EP, Barba P, De Rossi D. 2006 Wearable kinesthetic system for joint kneeflexion- extension monitoring in gait analysis. In2006 28th Annual Int. Conf. of the IEEEEngineering in Medicine and Biology Society, New York, NY, 30 August–3 September, vols 1–15,pp. 1579–1582. New York, NY: IEEE.

57. Lorussi F, Rocchia W, Scilingo EP, Tognetti A, De Rossi D. 2004 Wearable, redundant fabric-based sensor arrays for reconstruction of body segment posture.IEEE Sens. J.4, 807–818.(doi:10.1109/Jsen.2004.837498)

58. Carpi F, De Rossi D. 2005 Electroactive polymer-based devices for e-textiles in biomedicine(vol. 9, p. 295, 2005).IEEE Trans. Inf. Technol. Biomed.9, 574. (doi:10.1109/Titb.2005.858429)

59. De Rossi D, Carpi F, Scilingo EP. 2005 Polymer based interfaces as bioinspired 'smart skins'.Adv. Colloid Interface Sci.116, 165–178. (doi:10.1016/j.cis.2005.05.002)

60. Hu LB, Cui Y. 2012 Energy and environmental nanotechnology in conductive paper andtextiles.Energy Environ. Sci.5, 6423–6435. (doi:10.1039/C2ee02414d)

61. Chun KY, Oh Y, Rho J, Ahn JH, Kim YJ, Choi HR, Baik S. 2010 Highly conductive, printableand stretchable composite films of carbon nanotubes and silver.Nat. Nanotechnol.5, 853–857.(doi:10.1038/Nnano.2010.232)

62. Tang SLP. 2007 Recent developments in flexible wearable electronics for monitoringapplications.Trans. Inst. Meas. Control29, 283–300. (doi:10.1177/0142331207070389)

63. Siegel AC, Phillips ST, Dickey MD, Lu NS, Suo ZG, Whitesides GM. 2010 Foldableprinted circuit boards on paper substrates.Adv. Funct. Mater.20, 28–35. (doi:10.1002/adfm.200901363)

64. Park S, Mackenzie K, Jayaraman S. 2002 The wearable motherboard: a framework forpersonalized mobile information processing (PMIP). In39th Design Automation Conf., Proc.2002, New Orleans, LA, 10–14 January, pp. 170–174. New York, NY: IEEE.

65. Gopalsamy C, Park S, Rajamanickam R, Jayaraman S. 1999 The wearable motherboard:the first generation of adaptive and responsive textile structures (ARTS) for medicalapplications.Virtual Reality4, 152–168. (doi:10.1007/BF01418152)

66. Tognetti A, Lorussi F, Tesconi M, Bartalesi R, Zupone G, De Rossi D. 2006 Wearablekinesthetic systems for capturing and classifying body posture and gesture. In2005 27thAnnual Int. Conf. of the IEEE Engineering in Medicine and Biology Society, Shanghai, China, 17–18January, vols 1–7, pp. 1012–1015. New York, NY: IEEE.

67. Wu J, Zhou D, Too CO, Wallace GG. 2005 Conducting polymer coated lycra.Synth. Metals155, 698–701. (doi:10.1016/j.synthmet.2005.08.032)

68. Munro BJ, Campbell TE, Wallace GG, Steele JR. 2008 The intelligent knee sleeve: a wearablebiofeedback device.Sens. Actuators B, Chem.131, 541–547. (doi:10.1016/j.snb.2007.12.041)

69. Locher I, Trosler G. 2007 Screen-printed textile transmission lines.Text. Res. J.77, 837–842.(doi:10.1177/0040517507080679)

70. Chang HX, Wang GF, Yang A, Tao XM, Liu XQ, Shen YD, Zheng ZJ. 2010 A transparent,flexible, low-temperature, and solution-processible graphene composite electrode.Adv.Funct. Mater.20, 2893–2902. (doi:10.1002/adfm.201000900)

71. Zang JF, Ryu S, Pugno N, Wang QM, Tu Q, Buehler MJ, Zhao XH. 2013 Multifunctionalityand control of the crumpling and unfolding of large-area graphene.Nat. Mater.12, 321–325.(doi:10.1038/Nmat3542)

72. Sekitani T, Noguchi Y, Hata K, Fukushima T, Aida T, Someya T. 2008 A rubberlikestretchable active matrix using elastic conductors.Science321, 1468–1472. (doi:10.1126/science.1160309)

73. Chun KY, Kim SH, Shin MK, Kim YT, Spinks GM, Aliev AE, Baughman RH, Kim SJ. 2013Free-standing nanocomposites with high conductivity and extensibility.Nanotechnology24,165401. (doi:10.1088/0957-4484/24/16/165401)

74. Shang YY, Li YB, He XD, Zhang LH, Li Z, Li PX, Shi EZ, Wu ST, Cao AY. 2013 Elasticcarbon nanotube straight yarns embedded with helical loops.Nanoscale5, 2403–2410.(doi:10.1039/C3nr33633f)

75. Stoyanov H, Kollosche M, Risse S, Wache R, Kofod G. 2013 Soft conductive elastomermaterials for stretchable electronics and voltage controlled artificial muscles.Adv. Mater.25,578–583. (doi:10.1002/adma.201202728)
76. Teng C, Lu XY, Zhu Y, Wan MX, Jiang L. 2013 Polymer in situ embedding for highly flexible,stretchable and water stable PEDOT: PSS composite conductors.RSC Adv.3, 7219–7223.(doi:10.1039/C3ra41124a)
77. Yang C, Wong CP, Yuen MMF. 2013 Printed electrically conductive composites: conductivefiller designs and surface engineering.J. Mater. Chem. C1, 4052–4069. (doi:10.1039/C3tc00572k)
78. van der Sluis O, Timmermans PHM, van der Zanden EJL, Hoefnagels JPM. 2010 Analysisof the three-dimensional delamination behavior of stretchable electronics applications.Adv.Fract. Damage Mech. VIII417–418, 9–12.
79. Bossuyt F, Vervust T, Vanfleteren J. 2013 Stretchable electronics technology for large areaapplications: fabrication and mechanical characterization.IEEE Trans. Compon. Packag.Manuf. Technol.3, 229–235. (doi:10.1109/Tcpmt.2012.2185792)
80. Jones J, Lacour SP, Wagner S, Suo ZG. 2004 Stretchable wavy metal interconnects.J. VacuumSci. Technol. A22, 1723–1725. (doi:10.1116/1.1756879)
81. Lacour SP, Jones J, Wagner S, Li T, Suo ZG. 2005 Stretchable interconnects for elastic electronicsurfaces.Proc. IEEE93, 1459–1467. (doi:10.1109/Jproc.2005.851502)
82. Lacour SP, Jones J, Suo Z, Wagner S. 2004 Design and performance of thin metalfilm interconnects for skin-like electronic circuits.IEEE Electron Device Lett.25, 179–181.(doi:10.1109/Led.2004.825190)
83. Sun YG, Choi WM, Jiang HQ, Huang YGY, Rogers JA. 2006 Controlled buckling ofsemiconductor nanoribbons for stretchable electronics.Nat. Nanotechnol.1, 201–207. (doi:10.1038/nnano.2006.131)
84. Khang DY, Jiang HQ, Huang Y, Rogers JA. 2006 A stretchable form of single-crystalsilicon for high-performance electronics on rubber substrates.Science311, 208–212.(doi:10.1126/science.1121401)
85. Choi WM, Song JZ, Khang DY, Jiang HQ, Huang YY, Rogers JA. 2007 Biaxially stretchable‘wavy’ silicon nanomembranes.Nano Lett.7, 1655–1663. (doi:10.1021/Nl0706244)
86. Song J, Huang Y, Xiao J, Wang S, Hwang KC, Ko HC, Kim DH, Stoykovich MP, Rogers JA.2009 Mechanics of noncoplanar mesh design for stretchable electronic circuits.J. Appl. Phys.105, 123516. (doi:10.1063/1.3148245)

87. Song J, Jiang H, Huang Y, Rogers JA. 2009 Mechanics of stretchable inorganic electronicmaterials.J. Vacuum Sci. Technol. A27, 1107–1125. (doi:10.1116/1.3168555)
88. Ko HCet al. 2009 Curvilinear electronics formed using silicon membrane circuits andelastomeric transfer elements.Small5, 2703–2709. (doi:10.1002/smll.200900934)
89. Kim DHet al. 2008 Materials and noncoplanar mesh designs for integrated circuits withlinear elastic responses to extreme mechanical deformations.Proc. Natl Acad. Sci. USA105,18 675–18 680. (doi:10.1073/pnas.0807476105)
90. Kim RHet al. 2010 Waterproof AlInGaP optoelectronics on stretchable substrates withapplications in biomedicine and robotics.Nat. Mater.9, 929–937. (doi:10.1038/nmat2879)
91. Hu X, Krull P, de Graff B, Dowling K, Rogers JA, Arora WJ. 2011 Stretchableinorganic-semiconductor electronic systems.Adv. Mater.23, 2933–2936. (doi:10.1002/adma.201100144)
92. Kim RHet al. 2011 Stretchable, transparent graphene interconnects for arrays ofmicroscale inorganic light emitting diodes on rubber substrates.Nano Lett.11, 3881–3886.(doi:10.1021/nl202000u)
93. Xu F, Lu W, Zhu Y. 2011 Controlled 3D buckling of silicon nanowires for stretchableelectronics.ACS Nano5, 672–678. (doi:10.1021/Nn103189z)
94. White MSet al. 2013 Ultrathin, highly flexible and stretchable PLEDs.Nat. Photon.7, 811–816.(doi:10.1038/Nphoton.2013.188)
95. Shang SM, Zeng W, Tao XM. 2011 High stretchable MWNTs/polyurethane conductivenanocomposites.J. Mater. Chem.21, 7274–7280. (doi:10.1039/C1jm10255a)
96. Wakuda D, Suganuma K. 2011 Stretchable fine fiber with high conductivity fabricated byinjection forming.Appl. Phys. Lett.98, 073304. (doi:10.1063/1.3555433).
97. Sekitani T, Someya T. 2010 Stretchable, large-area organic electronics.Adv. Mater.22,2228–2246. (doi:10.1002/adma.200904054)
98. Zhou YC, Yao YG, Chen CY, Moon K, Wang H, Wong CP. 2014 The use of polyimide-modifiedaluminum nitride fillers in AlN@PI/Epoxy composites with enhanced thermal conductivityfor electronic encapsulation.Sci. Rep. UK4, 4779. (doi:10.1038/Srep04779)
99. Keplinger C, Sun JY, Foo CC, Rothemund P, Whitesides GM, Suo ZG. 2013 Stretchable,transparent, ionic conductors.Science341, 984–987. (doi:10.1126/science.1240228)
100. Lacour SP, Wagner S, Huang ZY, Suo Z. 2003 Stretchable gold conductors on elastomericsubstrates.Appl. Phys. Lett.82, 2404–2406. (doi:10.1063/1.1565683)

101. Gonzalez M, Axisa F, Bossuyt F, Hsu YY, Vandevelde B, Vanfleteren J. 2009 Design andperformance of metal conductors for stretchable electronic circuits.Circuit World35, 22–29.(doi:10.1108/03056120910928699)

102. Xiao J, Ryu SY, Huang Y, Hwang KC, Paik U, Rogers JA. 2010 Mechanics ofnanowire/nanotube in-surface buckling on elastomeric substrates.Nanotechnology21,085708. (doi:10.1088/0957-4484/21/8/085708)

103. Kim DH, Rogers JA. 2008 Stretchable electronics: materials strategies and devices.Adv. Mater.20, 4887–4892. (doi:10.1002/adma.200801788)

104. Vella D, Bico J, Boudaoud A, Roman B, Reis PM. 2009 The macroscopic delaminationof thin films from elastic substrates.Proc. Natl Acad. Sci. USA106, 10 901–10 906. (doi:10.1073/pnas.0902160106)

105. Jiang HQ, Sun YG, Rogers JA, Huang YG. 2008 Post-buckling analysis for the preciselycontrolled buckling of thin film encapsulated by elastomeric substrates (Reprinted Int. J. Solids Struct., vol. 45, pp. 2014–2023, 2008).Int. J. Solids Struct.45, 3858–3867.(doi:10.1016/S0020-7683(08)00168-6)

106. Wu J, Liu ZJ, Song J, Huang Y, Hwang KC, Zhang YW, Rogers JA. 2011 Stretchability ofencapsulated electronics.Appl. Phys. Lett.99, 061911 (doi:10.1063/1.3624848)

107. Lam SW, Xue P, Tao XM, Yu TX. 2003 Multi-scale study of tensile properties and largedeformation mechanisms of polyethylene terephthalate/polypropylene knitted composites.Compos. Sci. Technol.63, 1337–1348. (doi:10.1016/S0266-3538(02)00077-5)

108. Brosteaux D, Axisa F, Gonzalez M, Vanfleteren J. 2007 Design and fabrication of elasticinterconnections for stretchable electronic circuits.IEEE Electron Device Lett.28, 552–554.(doi:10.1109/Led.2007.897887)

109. Lee J, Chung S, Song H, Kim S, Hong Y. 2013 Lateral-crack-free, buckled, inkjet-printed silverelectrodes on highly pre-stretched elastomeric substrates.J. Phys. D, Appl. Phys.46, 105305.(doi:10.1088/0022-3727/46/10/105305)

110. Ryu SY, Xiao JL, Il Park W, Son KS, Huang YY, Paik U, Rogers JA. 2009 Lateralbuckling mechanics in silicon nanowires on elastomeric substrates.Nano Lett.9, 3214–3219.(doi:10.1021/Nl901450q)

111. Ho XN, Tey JN, Liu WJ, Cheng CK, Wei J. 2013 Biaxially stretchable silver nanowiretransparent conductors.J. Appl. Phys.113, 044311. (doi:10.1063/1.4789795)

112. Lee Jet al. 2013 Room-temperature nanosoldering of a very long metal nanowire network byconducting-polymer-assisted joining for a flexible touch-panel application.Adv. Funct. Mater.23, 4171–4176. (doi:10.1002/adfm.201203802)

113. Zhu S, So JH, Mays R, Desai S, Barnes WR, Pourdeyhimi B, Dickey MD. 2013 Ultrastretchablefibers with metallic conductivity using a liquid metal alloy core.Adv. Funct. Mater.23,2308–2314. (doi:10.1002/adfm.201202405)
114. Liang JJ, Li L, Niu XF, Yu ZB, Pei QB. 2013 Elastomeric polymer light-emitting devices anddisplays.Nat. Photon.7, 817–824. (doi:10.1038/Nphoton.2013.242)
115. Zeng W, Shu L, Li Q, Chen S, Wang F, Tao XM. 2014 Fiber-based wearable electronics:a review of materials, fabrication, devices and applications.Adv. Mater.(doi:10.1002/adma.201400633)
116. Cao W. 2013 Fabrication and modeling of stretchable conductors for traumatic brain injuryresearch. 213 pp. Department of Electrical Engineering, Princeton University.
117. Wang SD, Xiao JL, Song JZ, Ko HC, Hwang KC, Huang YG, Rogers JA. 2010 Mechanics ofcurvilinear electronics.Soft Matter6, 5757–5763. (doi:10.1039/C0sm00579g)
118. Leaf GAV. 1958 A property of a buckled elastic rod.Br. J. Appl. Phys.9, 71–72.(doi:10.1088/0508-3443/9/2/305)
119. Atanackovic TM. 1997Stability theory of elastic rods, xiii, 425 pp. Singapore: World Scientific.
120. Romeo A, Liu QH, Suo ZG, Lacour SP. 2013 Elastomeric substrates with embedded stiffplatforms for stretchable electronics.Appl. Phys. Lett.102, 131904. (doi:10.1063/1.4799653)
121. Someya T. 2013Stretchable electronics. (pp. 1 online resource (xxi, 462 p.). Weinheim, Germany:Wiley-VCH.
122. Wang YY, Hua T, Zhu B, Li Q, Yi WJ, Tao XM. 2011 Novel fabric pressure sensors: design,fabrication, and characterization.Smart Mater. Struct.20, 065015 (doi:10.1088/0964-1726/20/6/065015)
123. Kim DHet al. 2008 Stretchable and foldable silicon integrated circuits.Science320, 507–511.(doi:10.1126/science.1154367)
124. Kinkeldei T, Munzenrieder N, Zysset C, Cherenack K, Troster G. 2011 Encapsulationfor flexible electronic devices.IEEE Electron Device Lett.32, 1743–1745. (doi:10.1109/Led.2011.2168378)
125. Khang DY, Rogers JA, Lee HH. 2009 Mechanical buckling: mechanics, metrology, andstretchable electronics.Adv. Funct. Mater.19, 1526–1536. (doi:10.1002/adfm.200801065)
126. Au KF. 2011Advances in knitting technology. Woodhead Publishing Series in Textiles.Cambridge, UK: Woodhead Publishing and the Textile Institute.

127. Beckmann L, Neuhaus C, Medrano G, Jungbecker N, Walter M, Gries T, Leonhardt S.2010 Characterization of textile electrodes and conductors using standardized measurementsetups.Physiol. Meas.31, 233–247. (doi:10.1088/0967-3334/31/2/009).
128. Fjelstad J. 1998Flexible circuit technology, 2nd edn, 217 pp. Sunnyvale, CA: Silicon ValleyPublishers Group.
129. Ray SC. 2012 Fundamentals and advances in knitting technology. InWoodhead publishingIndia in textiles. New Delhi, India: Woodhead Pub. India Pvt.

Electronic supplementary material

Three-dimensionally Deformable, Highly Stretchable, Permeable, Durable and Washable Fabric Circuit Boards

*Qiao Li[1], and Xiao Ming Tao[1,2]**

[1]Institute of Textiles and Clothing, [2]Interdisciplinary Division of Biomechanical Engineering, The Hong Kong Polytechnic University, Hong Kong
*E-mail: xiao-ming.tao@polyu.edu.hk

1. Selection of fabric structure

Textile fabrics, including woven, knitting and nonwoven, are thin (~<1mm), lightweight (~grams per square meter), soft (Young's modulus: <1MPa), drapable in three dimensions, as well as porous (or breathable), are attractive to be used as flexible substrates or circuit boards for wearable electronics on human bodies. As illustrated in Fig.S2, a plain woven fabric is produced by interlacing warp (along the length) and weft yarns (along the width of the fabric) at right angles to each other; a nonwoven fabric is made from long fibers, bonded together by chemical, mechanical, heat treatment. Unlike woven and nonwoven textiles, knitted fabric is formed by interlacing yarn in a series of connected loops, where the column and row directions of the loop are referred to as wale and course, respectively. Thus, the knitted fabric, especially weft knitting, in comparison to woven and nonwoven textiles, is much more elastic (usually beyond 100% strain) owing to its three-dimensional loop configuration. Hence, the efforts to develop knitted FCBs may open doors to new applications in areas where woven and nonwoven electronic devices are not effective, such as intimately wearable electronics or next-to-skin health monitoring network or system.

2. 3D loop configuration based on Leaf's model

Suppose a textile yarn in the knitted fabric as a thin elastic rod. Define yarn axis as a space curve in a rectangular Cartesian coordinate system. The position of a generic point on the yarn axis in the natural state was determined by employing Leaf's model for dry-relaxed plain knitted fabrics, i.e., a two-dimensional knitted fabric is firstly created by joining thin elastic rods end to end. The third dimension is then obtained by placing the two-dimensional model on a sine wave-like surface of a cylinder, whose generators are parallel to the line of courses. Thus, the loop configuration of the yarn axis could be expressed by

$$\left.\begin{aligned} x &= b\{2E(\varphi,\varepsilon) - F(\varphi,\varepsilon)\} \\ y &= p(\frac{\pi}{2} - \psi) \\ z &= q(\sin\psi - 1) \end{aligned}\right\}$$

, where $0 \le \varphi \le \pi/2$, $0 \le \psi \le \pi/2$, ε is constant, i.e., $\varepsilon = 0.8090$, and $F(\varphi,\varepsilon)$, $E(\varphi,\varepsilon)$ are incomplete elliptic integrals of the first and second kinds, respectively. The equation

$$\cos\varphi = 1 - \frac{E(\psi, w)}{E(\pi/2, w)}$$

relates the parameters φ and ψ . And the parameters *p*, *q*, *b* would be completely determined by the equations

$$\left.\begin{aligned} l &= 4bF(\frac{\pi}{2},\varepsilon) \\ 2b\varepsilon &= \frac{q}{w}E(\frac{\pi}{2}, w) \\ w^2 &= \frac{q^2}{p^2 + q^2} \\ \cos\varphi &= 1 - \frac{E(\psi, w)}{E(\frac{\pi}{2}, w)} \end{aligned}\right\}$$

once the loop length l is obtained. Same to ε, w is constant, i.e., $w = 0.5766$. The loop length l can be determined from Munden's observation for experimental results, that is,

$$\left.\begin{aligned} C \times W &= K_1 / l^2 \\ C &= K_2 / l \\ W &= K_3 / l \end{aligned}\right\}$$

, where C and W are, respectively, the number of courses and wales per unit length, and K_1, K_2 and K_3 are constants. For dry-relaxed fabrics, they are $K_1 = 19.0$, $K_2 = 5.0$ and $K_3 = 3.8$.

3. Fabrication and characterization of fabric sensing network as smart protective vest

3.1 Fabrication of helical connection

As depicted in Fig.S9, the detailed procedures for the helical connection between the sensor electrode and the metal fibers in the knitted FCB are as follows: 1) polyurethane film of the metal fiber was removed; 2) sensor electrode was twisted with the naked metal fiber in the knitted FCB; 3) silicone-based electrically conductive adhesive Silductor 6310 was injected into the twisted region; 4) the twisted part was wrapped around one stainless steel needle (diameter: ~1mm) to make a circular helix; 5) A semi-spherical encapsulation was made by a mould.

3.2 In-situ measurement by smart protective vest during ballistic impact

The primary specifications for the ballistic impact test are listed in Table S2. The impact test was conducted at a mean temperature of ~23℃. The base material, integrated with the fabric sensing network, was first plugged into piles of multiple sheets of the energy absorbing materials. Then, all the sheets were tied on the surface of a foundation, i.e. clay, with marked locations of the sensors on the front ply. Next, the knitted FCB assemblies were connected to data acquisition equipment (DEWE-2600, S/N28110201) (Fig.S12). Finally, a bullet (diameter: 7.62mm, weight:

~4.7g) was impacted at the centre of the sensor array on the energy absorbing material pile and made an indentation into the foundation clay. The impact velocity was 295-305m.s^{-1}. In the impact process, the electrical resistance of the sensors was recorded by the data acquisition equipment with a sampling rate of 100 kHz.

Table S1. Physical properties of the dielectric supporting materials in the knitted FCB.

Properties	**Polyamide**	**Spandex**
Density (g/cm^3)	1.15	1.15-1.32
Elastic modulus (MPa)	2100-3400	
Poisson's ratio	0.4	0.862
Elongation (%)	200	400-700
Tensile strength (MPa)	75	
Thermal conductivity (W/(m.k))	0.25	
Melting point (℃)	190-350	250
Linear expansion coefficient (/k)	4×10^{-5}	
Electrical conductivity (S/m)	10^{-12}	Insulate
Dielectric constant	3.5	
Water absorption (%)	0.5-0.6	0.8-1.2

Table S2. Specifications for the ballistic impact test.

Place	Ballistic Research Laboratory, School of Power Engineering, Nanjing University of Science and Technology
Materials and impact speed	Plies: UHMWPE/Kevlar; Foundations: clay and gelatin; Gun and bullet: Type-77/316/handgun, Type-64/7.62mm/handgun common cartridges; Impact speed: 295-305m/s
Procedures	1. Fix a single ply of UMMWPE/Kevlar integrated with the evaluation system into the multi-plies of ballistic material; 2. Mark the locations of sensors on the front ply; 3. Set up the foundation material on a table; 4. Tie the multi-plies of ballistic material onto the surface of foundation material with transparent adhesive tape; 5. Connect wires with the fabric FCB and data acquisition equipment; 6. Establish and debug the high-speed digital video recorder; 7. Take a bullet shooting, while strains being measured and impact process being videoed; 8. Record the point of bullet impact, investigate the damage of ballistic material, and measure the deformation of foundation.

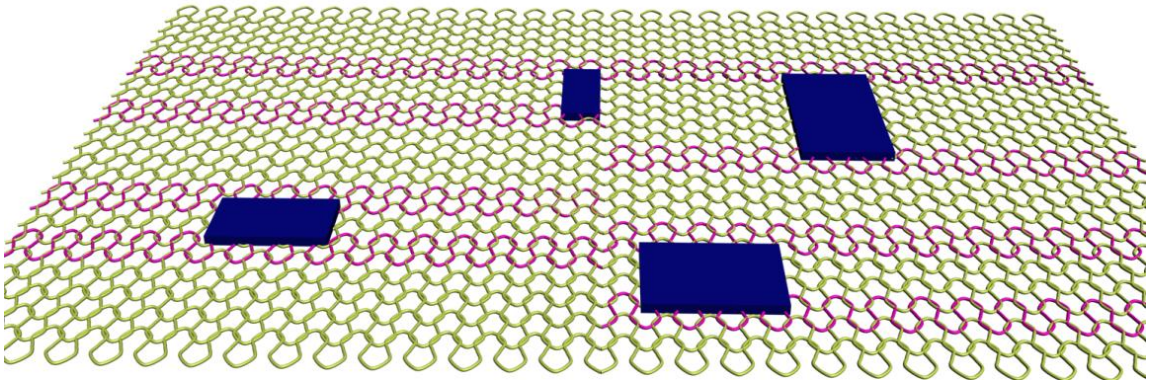

(a)

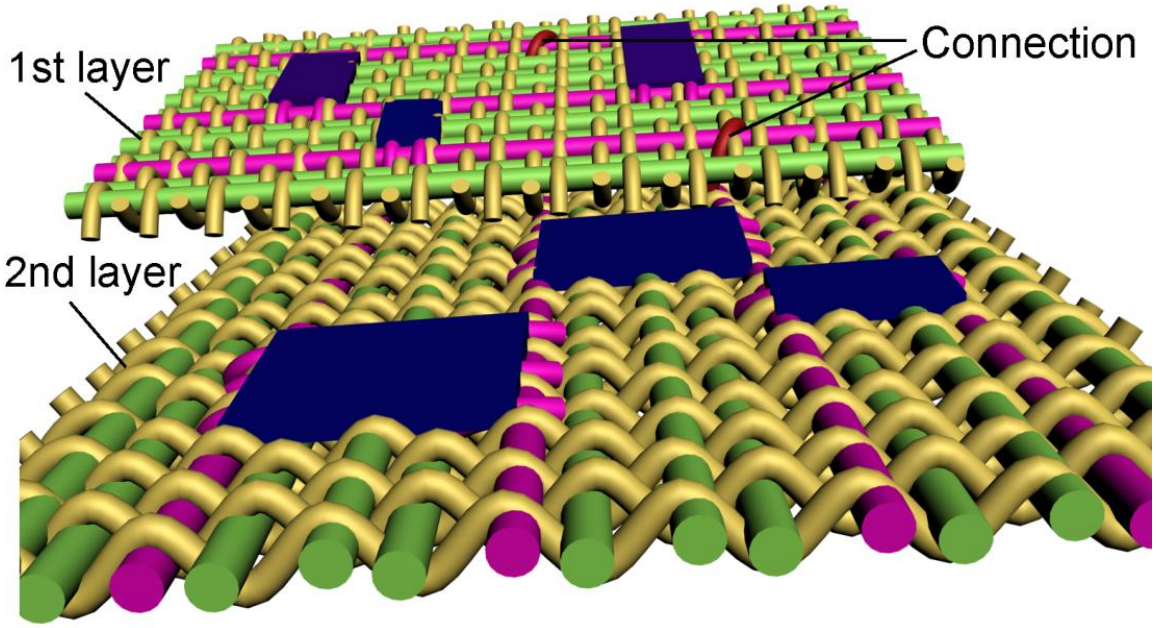

(b)

Figure S1. Single- (a) and double- (b) layered FCBs.

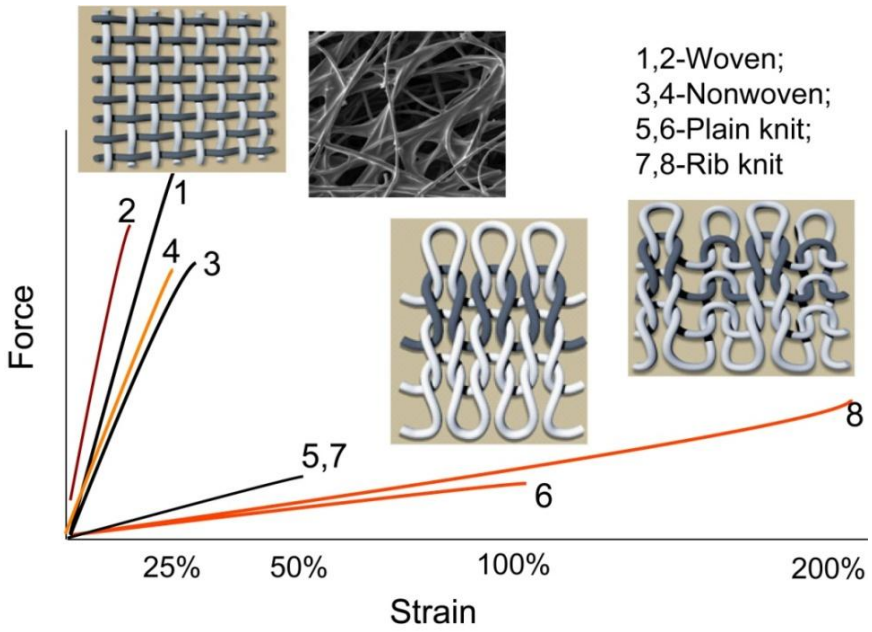

(a)

Figure S2. Mechanical properties of different textile structures.

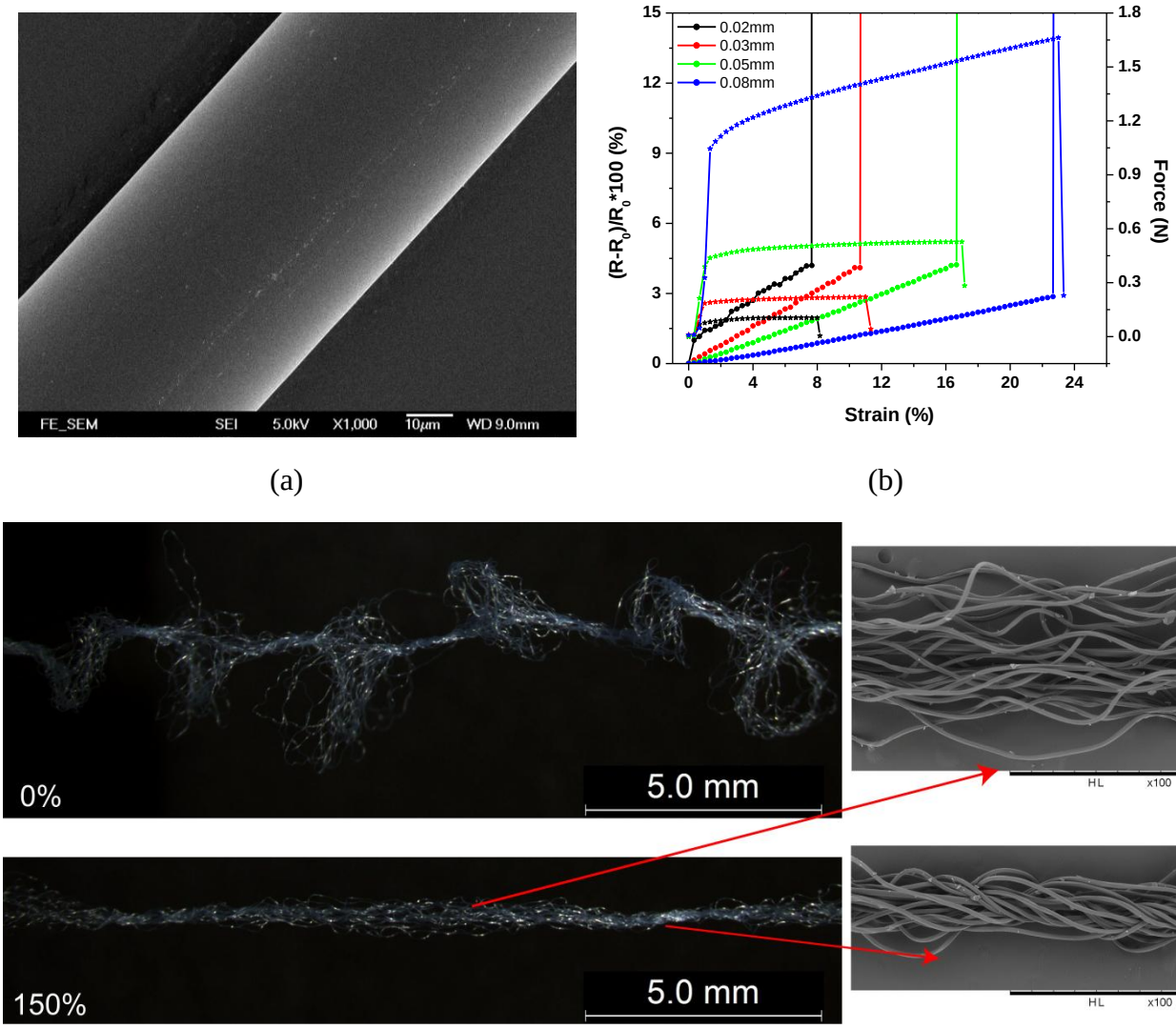

(a) (b)

(c)

Figure S3. Materials of the knitted FCB. (a) SEM images of the coated metal fibers (core diameter: ~50μm; coating thickness: ~3μm). (b) Electro-mechanical properties of the coated metal fibers with different core diameters (from 20 μm to 80 μm). (c) Microstructure of the textured filament yarn.

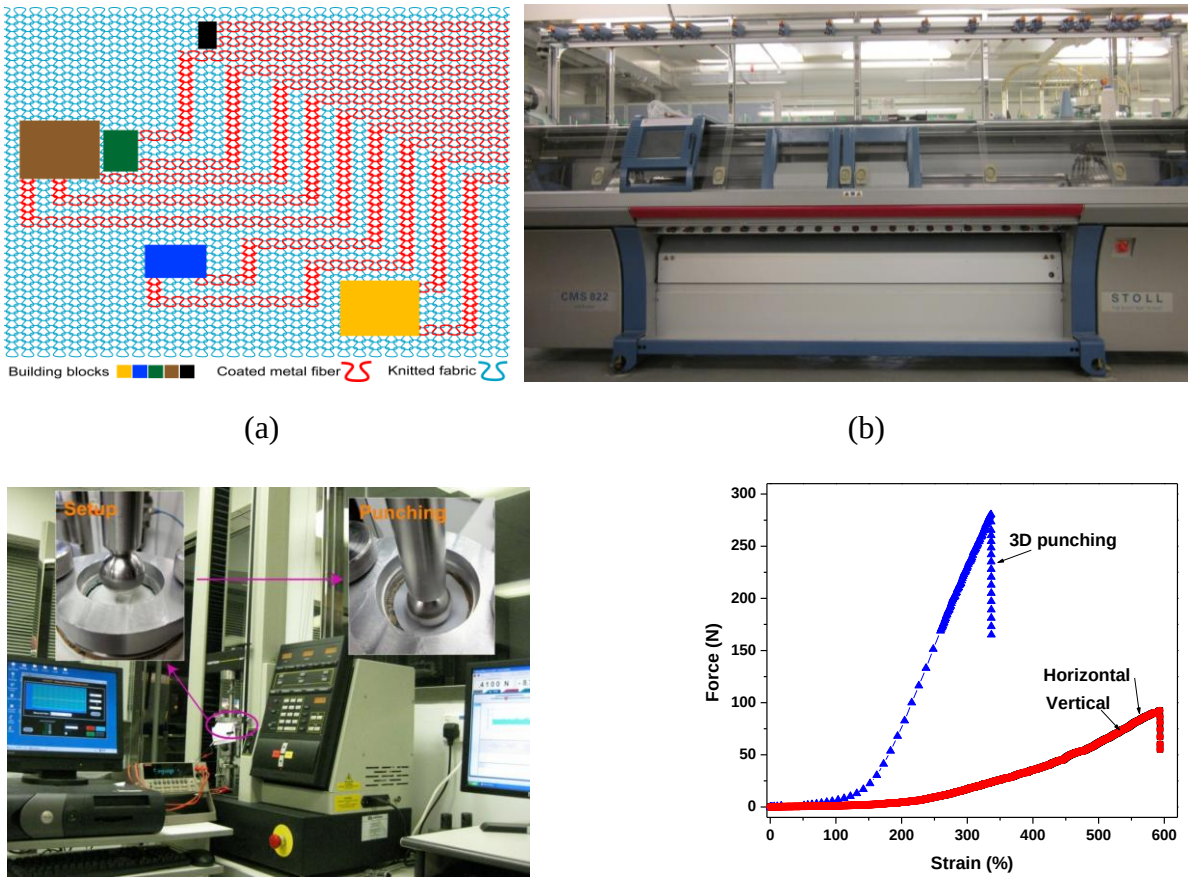

(a) (b)

(c) (d)

Figure S4. Fabrication and characterization of the knitted FCB. (a) Computerized design of a circuit diagram. (b) Computerized flat-bed knitting machine. (c) Experimental setup for a 3D ball punching test. (d) Mechanical performance of the resulting knitted FCB.

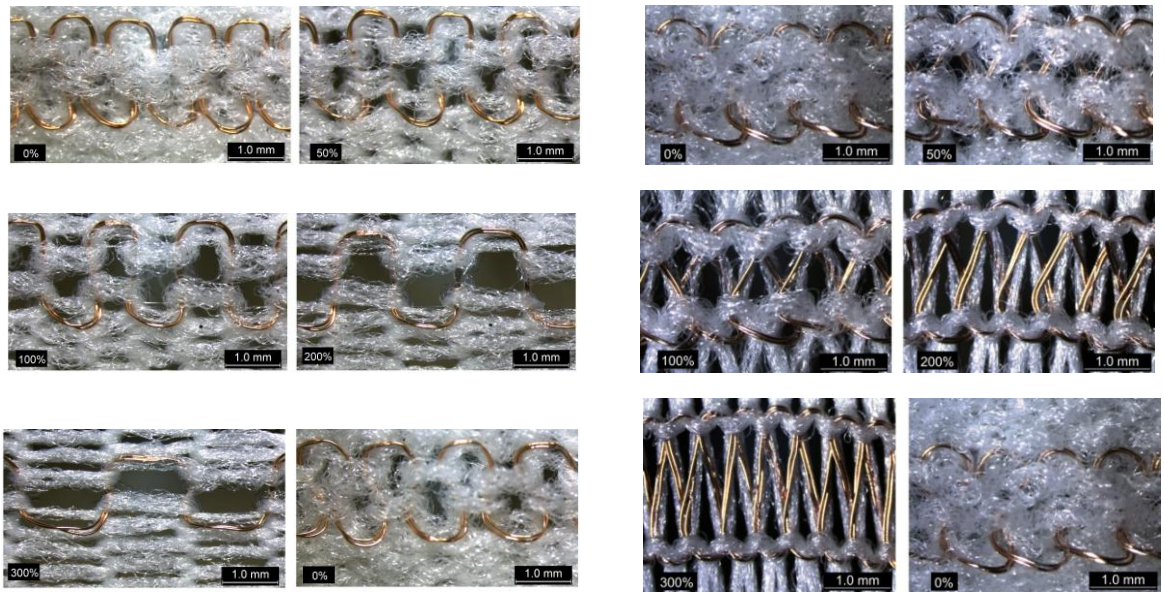

(a) (b)

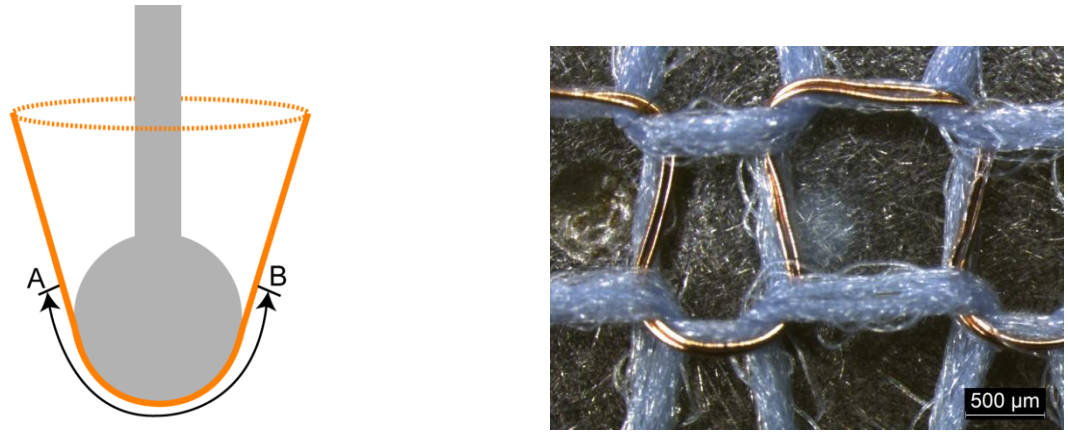

(c)

Figure S5. Optical images of the knitted FCB with applied strain in transverse (a), longitudinal (b) tensile and 3D ball punching tests (c).

(a)

(b)

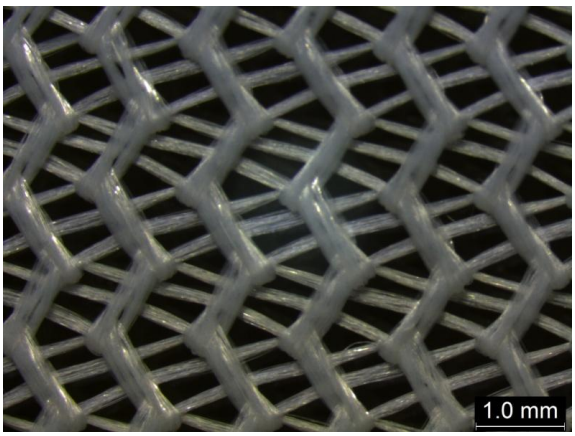

(c)

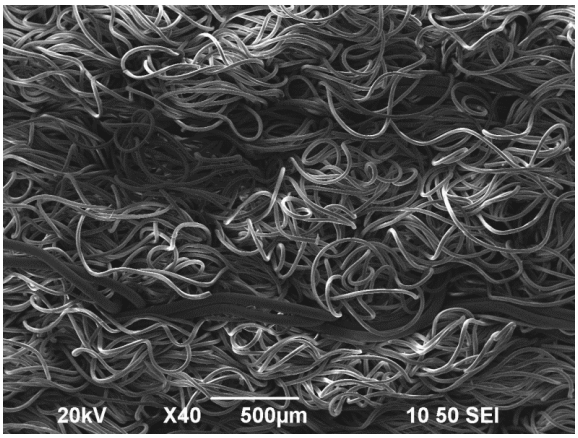

(d)

Figure S6. Washing test of the knitted FCB. (a)-(b) Washing machine with different cycles. (c) Microcopic image of the mesh bag. (d) SEM image of FCB sample with electrical integrity after 30 times' washing.

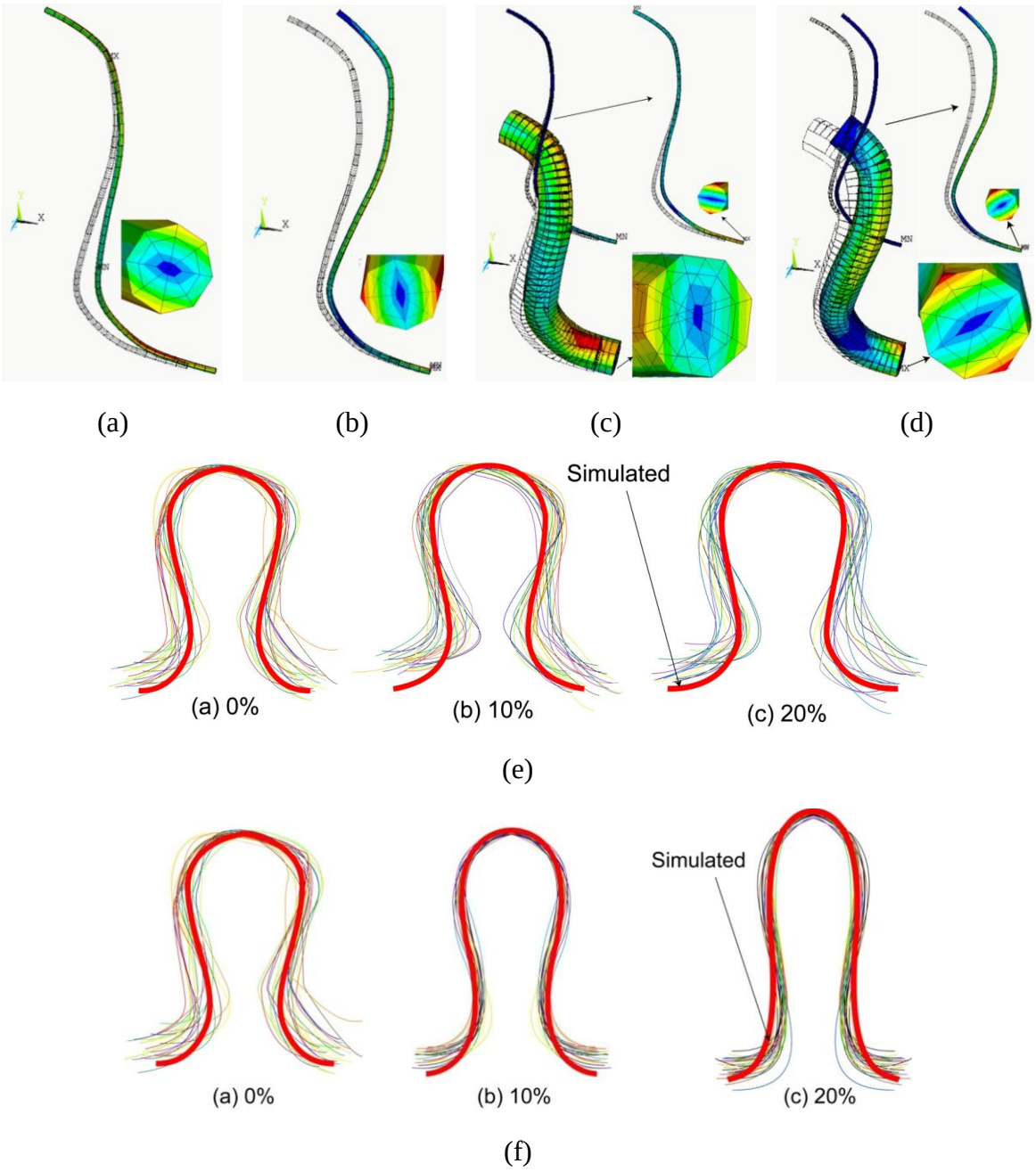

Figure S7. Finite element simulation of the knitted FCB in tensile test. (a)-(b) Strain distribution for a free-standing looped metal fiber at 20% FCB elongation in transverse and longitudinal cases, respectively. (c)-(d) Strain distribution for a looped metal fiber interlaced with a textile filament in transverse and longitudinal directions, respectively. (e)-(f) Comparison with experimental observations in the transverse and longitudinal tensile tests, respectively.

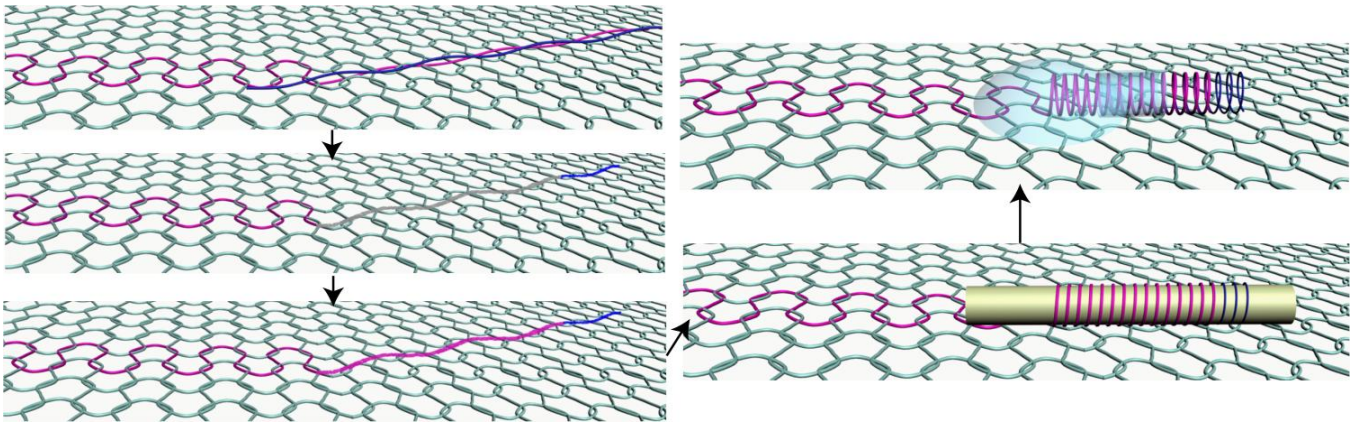

Figure S8. Process flow for fabrication of the helical connection.

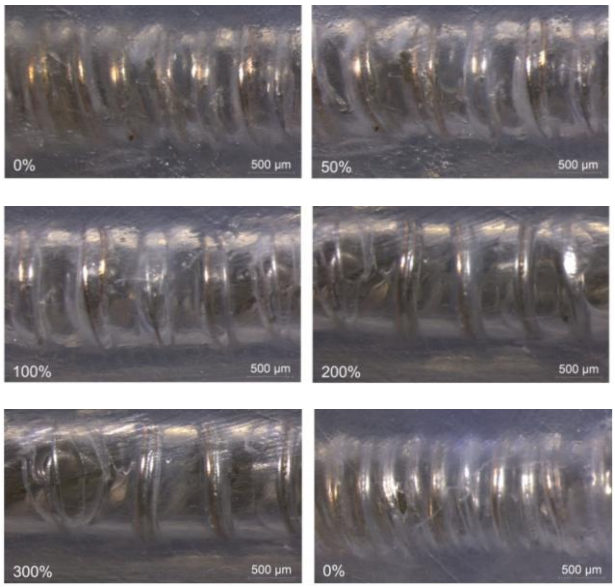

(a)

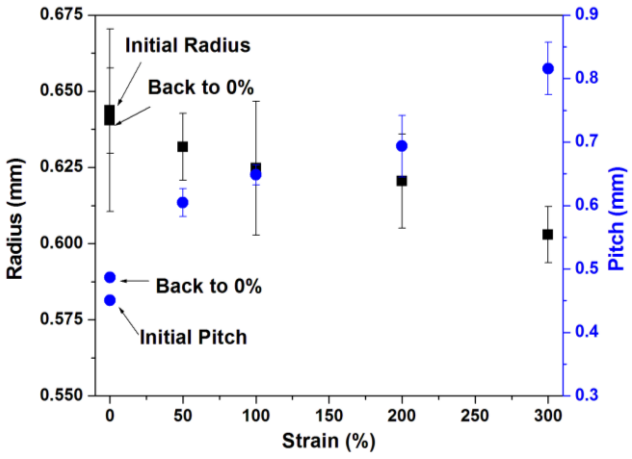

(b)

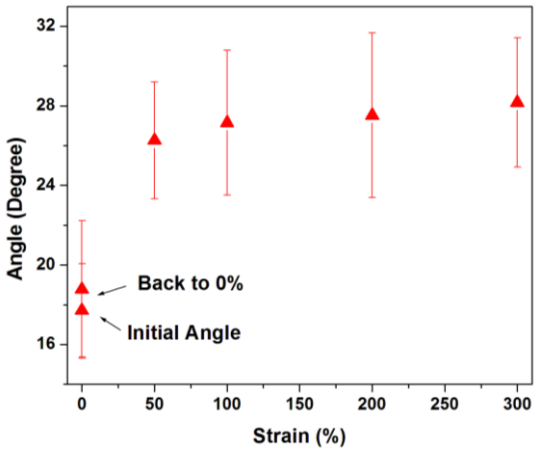

(c)

Figure S9. Geometrical change of the helical connection with applied tensile strain. (a) Optical images of the helical connection with applied strain. (b)-(c) In-plane radius, pitch and angle with applied strain.

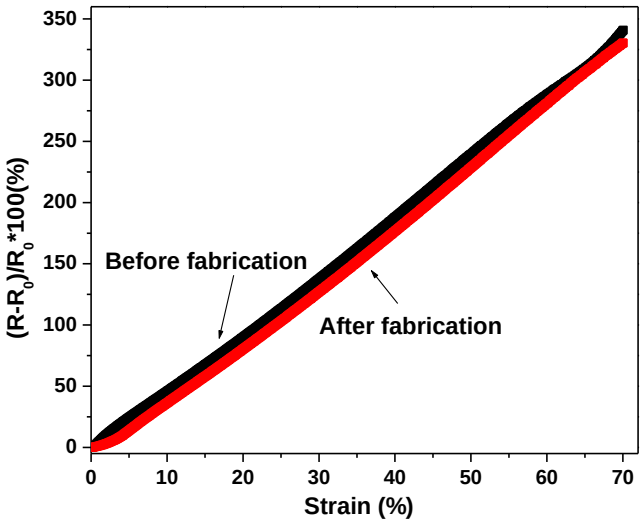

Figure S10. Electro-mechanical property of one sensor element before and after fabrication of the fabric sensing network.

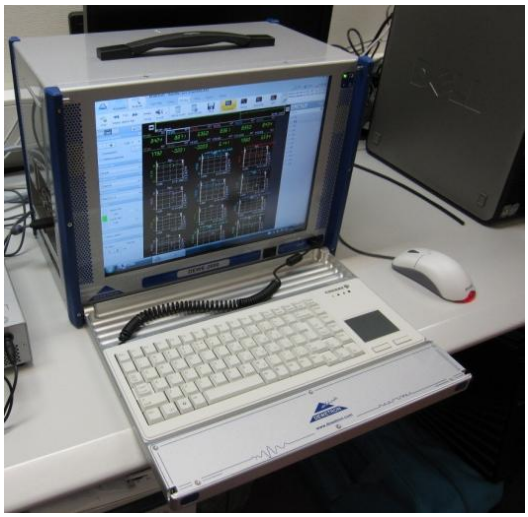

Figure S11. Data acquisition equipment for in-situ ballistic impact measurement.